www.nature.com/cr
www.cell-research.com

ARTICLE

SCUBE2 mediates bone metastasis of luminal breast cancer by modulating immune-suppressive osteoblastic niches

Qiuyao Wu[1], Pu Tian[1], Dasa He[1], Zhenchang Jia[1], Yunfei He[1], Wenqian Luo[1], Xianzhe Lv[1], Yuan Wang[1], Peiyuan Zhang[1], Yajun Liang[1], Wenjin Zhao[2], Jun Qin[1], Peng Su[3], Yi-Zhou Jiang[4], Zhi-Ming Shao[4], Qifeng Yang[5]✉ and Guohong Hu[1]✉

Estrogen receptor (ER)-positive luminal breast cancer is a subtype with generally lower risk of metastasis to most distant organs. However, bone recurrence occurs preferentially in luminal breast cancer. The mechanisms of this subtype-specific organotropism remain elusive. Here we show that an ER-regulated secretory protein SCUBE2 contributes to bone tropism of luminal breast cancer. Single-cell RNA sequencing analysis reveals osteoblastic enrichment by SCUBE2 in early bone-metastatic niches. SCUBE2 facilitates release of tumor membrane-anchored SHH to activate Hedgehog signaling in mesenchymal stem cells, thus promoting osteoblast differentiation. Osteoblasts deposit collagens to suppress NK cells via the inhibitory LAIR1 signaling and promote tumor colonization. SCUBE2 expression and secretion are associated with osteoblast differentiation and bone metastasis in human tumors. Targeting Hedgehog signaling with Sonidegib and targeting SCUBE2 with a neutralizing antibody both effectively suppress bone metastasis in multiple metastasis models. Overall, our findings provide a mechanistic explanation for bone preference in luminal breast cancer metastasis and new approaches for metastasis treatment.

Cell Research (2023) 33:464–478; https://doi.org/10.1038/s41422-023-00810-6

INTRODUCTION

Metastasis to bone, brain, lung and other visceral organs accounts for the majority of deaths in breast cancer patients.[1] Among these target organs, bone is the most frequent metastasis site of breast cancer.[2] More than 70% of late-stage breast cancer patients develop bone metastasis, causing severe bone pain, fracture and lethal complications.[3,4] Since the molecular subtypes of breast cancer were described,[5] a number of studies reported the differences in prognosis,[6,7] chemotherapy response[8] and metastasis tendency[9,10] of different subtypes. The association between tumor subtypes and sites of distant relapse has also come into the spotlight recently.[11,12] Clinical studies showed that the preferences for bone metastasis among various subtypes are directly related to the expression of ER.[9–14] Bone metastasis tends to occur in luminal breast cancer, especially the ER^+ tumors[9,10,14–17]; however, the risk of metastasis to non-bone organs is significantly lower in luminal cancer than in other subtypes.[12] Previously some studies have identified the association between certain regulatory pathways and bone metastasis in luminal breast cancer,[18,19] but the molecular mechanisms that drive this target organ selectivity remain elusive.

The development and outgrowth of bone metastasis depend on the intricate cellular and molecular interactions between cancer cells and stromal components in the bone.[3] In particular, the ability of tumor cells to disrupt the bone homeostasis maintained by two types of resident cells, osteoclasts and osteoblasts, has been shown to drive bone destruction and metastatic growth.[20] Many studies have firmly demonstrated the critical roles of osteoclasts in metastatic outgrowth of breast cancer in bone.[3,21,22] The vicious cycle of mutual interactions between tumor and osteoclasts seems indispensable for breast-to-bone metastasis, and agents that suppress osteoclast activity have come into clinical use.[17,23] However, osteoclast-targeting treatments can only alleviate the progression of metastasis, but not effectively improve the survival of patients.[17,24,25] Recent studies also suggested osteogenic cells as key components in early bone colonization of breast cancer.[26–32] Osteogenic niche facilitates bone metastasis by directly promoting proliferation of cancer cells or by engaging osteoclasts to foster the osteolytic microenvironment.[28–32] Osteoblasts are also suggested to be involved in maintenance of tumor dormancy.[33] However, the regulation of osteoblasts by cancer cells and the involvement of osteoblasts in bone metastasis of luminal breast cancer are still unclear. Importantly, most previous studies on bone metastasis of breast cancer are conducted with triple-negative breast cancer models, and little is known about the mechanisms for the bone proclivity of ER^+ luminal breast cancer in metastasis.

SCUBE2 is a member of the signal peptide-CUB domain-EGF-related (SCUBE) gene family.[34] The function of SCUBE2 was first identified in zebrafish with a non-cell-autonomous role in long-range Hedgehog signaling.[35–37] Later research in mouse and human found that SCUBE2 mediates the release of plasma membrane-bound Hedgehog ligands.[38] All morphogens of the Hedgehog family are synthesized as dual-lipidated proteins firmly

[1]Shanghai Institute of Nutrition and Health, University of Chinese Academy of Sciences, Chinese Academy of Sciences, Shanghai, China. [2]Pathology Tissue Bank, Qilu Hospital of Shandong University, Ji'nan, Shandong, China. [3]Department of Pathology, Qilu Hospital of Shandong University, Ji'nan, Shandong, China. [4]Department of Breast Surgery, Precision Cancer Medicine Center, Fudan University Shanghai Cancer Center, Shanghai, China. [5]Department of Breast Surgery, Qilu Hospital of Shandong University, Ji'nan, Shandong, China. ✉email: qifengy@163.com; ghhu@sinh.ac.cn

Received: 18 October 2022 Accepted: 2 April 2023
Published online: 4 May 2023

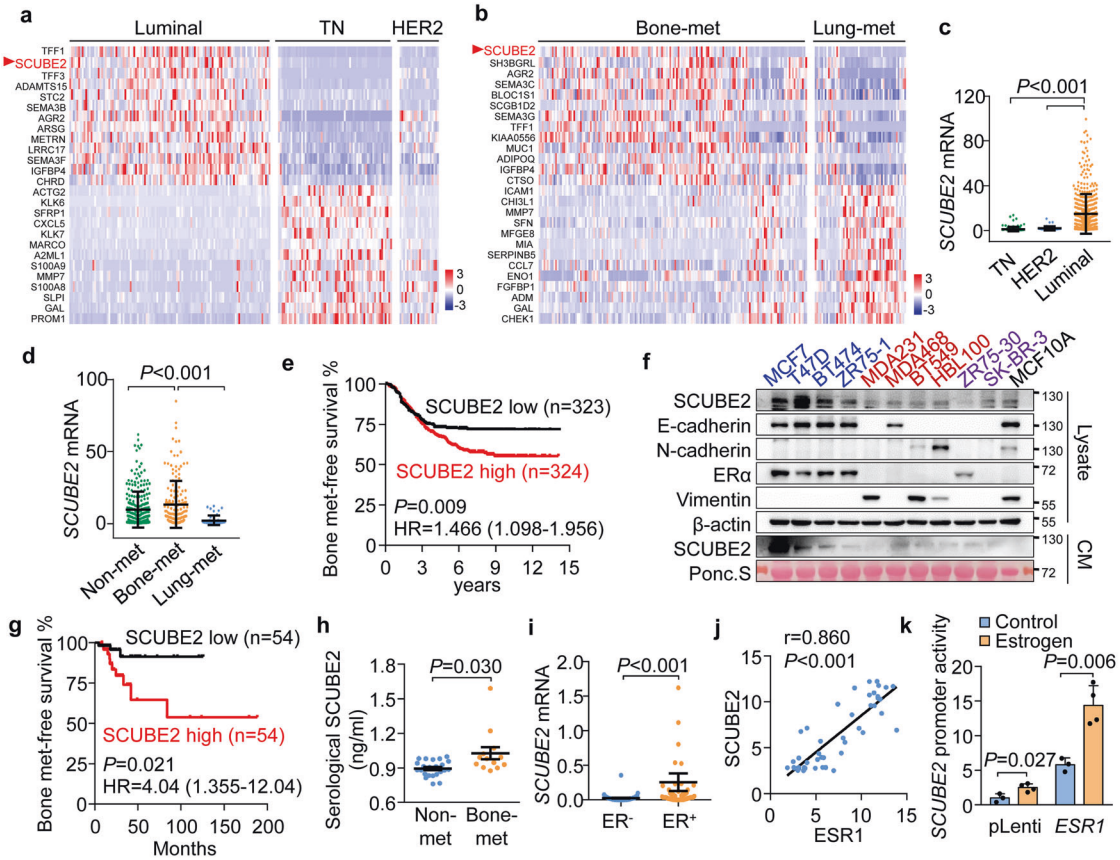

Fig. 1 SCUBE2 correlates with bone metastasis and is regulated by ER signaling in luminal breast cancer. a, **b** Expression heatmap of secretory protein-encoding genes differentially expressed in breast cancer patients with different molecular subtypes (**a**) and metastasis organotropism (**b**) in the merged Erasmus/MSK cohort.[46–49] Columns represent patients and rows represent genes. TN, triple negative tumors. **c**, **d** *SCUBE2* mRNA levels in Erasmus/MSK patients with different subtypes (**c**) and metastasis organotropism (**d**). **e** Bone metastasis-free survival analyses of Erasmus/MSK patients of all subtypes stratified by *SCUBE2* expression. **f** SCUBE2 expression and secretion levels in luminal (blue), TN (red), HER2$^+$ (purple) cancer and normal (black) mammary cell lines. **g** Bone metastasis-free survival analyses of the Qilu breast cancer patients stratified by *SCUBE2* mRNA levels of primary tumors. **h** Serological SCUBE2 levels of Qilu patients with different metastatic status ($n = 23$, 13 for non-met and bone-met, respectively). **i** *SCUBE2* mRNA expression in Qilu tumors grouped by ER status ($n = 51$, 57 for ER$^-$ and ER$^+$, respectively). **j** Correlation between SCUBE2 and ESR1 expression in the GSE3744 patient dataset.[51] **k** *SCUBE2* promoter activity in T47D cells with *ESR1* overexpression and/or estrogen treatment ($n = 3$ biologically independent samples). HR, hazard ratio. *P* values were calculated by two-tailed unpaired *t*-test (**c**, **d**, **h**, **i**, **k**), log-rank test (**e**, **g**) or Pearson correlation analysis (**j**). Data represent mean ± SD (**c**, **d**, **k**) or mean ± SEM (**h**, **i**).

attached to the surface of the cells in which they are produced.[39] SCUBE2 is involved in proteolytic release of membrane-anchored Sonic Hedgehog (SHH),[40] promoting its solubility in the extracellular space[41,42] and enhancing the interaction of SHH with its receptor PTCH1.[43,44] SCUBE2 is reported in a gene panel associated with breast cancer bone metastasis,[45] but its function and mechanism in bone metastasis are largely unclear. Here we show the stromal cell atlas at the early stage of bone colonization of luminal breast cancer, and report that SCUBE2 promotes bone metastasis by regulating osteoblast differentiation and immune suppression in metastatic niches.

RESULTS

SCUBE2 is upregulated in luminal breast cancer and correlates with bone metastasis

Reasoning that luminal-specific molecules might underlie the bone preference of luminal cancer, we analyzed several public gene expression datasets of clinical breast tumors and cell lines to search for candidate genes associated with both luminal subtype and bone metastasis. We focused on genes encoding secreted proteins since tumor–microenvironment interaction plays a crucial role in metastasis organotropism and tumor-secreted proteins are major mediators for such interaction. We first analyzed a public Erasmus/MSK clinical dataset[46–49] with information on both molecular subtyping and organ-specific metastasis. The analysis revealed a plethora of luminal-specific or bone metastasis-specific genes (Fig. 1a, b). Notably, *SCUBE2*, encoding a secretory protein, appeared as a top candidate in both the genes upregulated in luminal tumors vs other subtypes (Fig. 1a) and the genes upregulated in bone-metastatic tumors vs lung-metastatic tumors (Fig. 1b). In addition, *SCUBE2* was also one of the top luminal-specific genes in the Cancer Genome Atlas clinical dataset[50] (Supplementary information, Fig. S1a) and a public gene expression dataset (GSE10890) of breast cancer cell lines (Supplementary information, Fig. S1b). In these cohorts, *SCUBE2* was highly expressed in luminal tumors, but not in triple-negative or HER2$^+$ tumors, or normal tissues (Fig. 1c; Supplementary information, Fig. S1c). *SCUBE2* was also upregulated in bone-metastatic tumors compared to non-metastatic or lung-metastatic tumors (Fig. 1d). Kaplan-Meier survival analysis demonstrated the positive correlation of *SCUBE2* expression with risk of bone metastasis in the whole cohort (Fig. 1e). In luminal tumors, SCUBE2 was also linked to metastasis to bone, but not to visceral organs (Supplementary information, Fig. S1d).

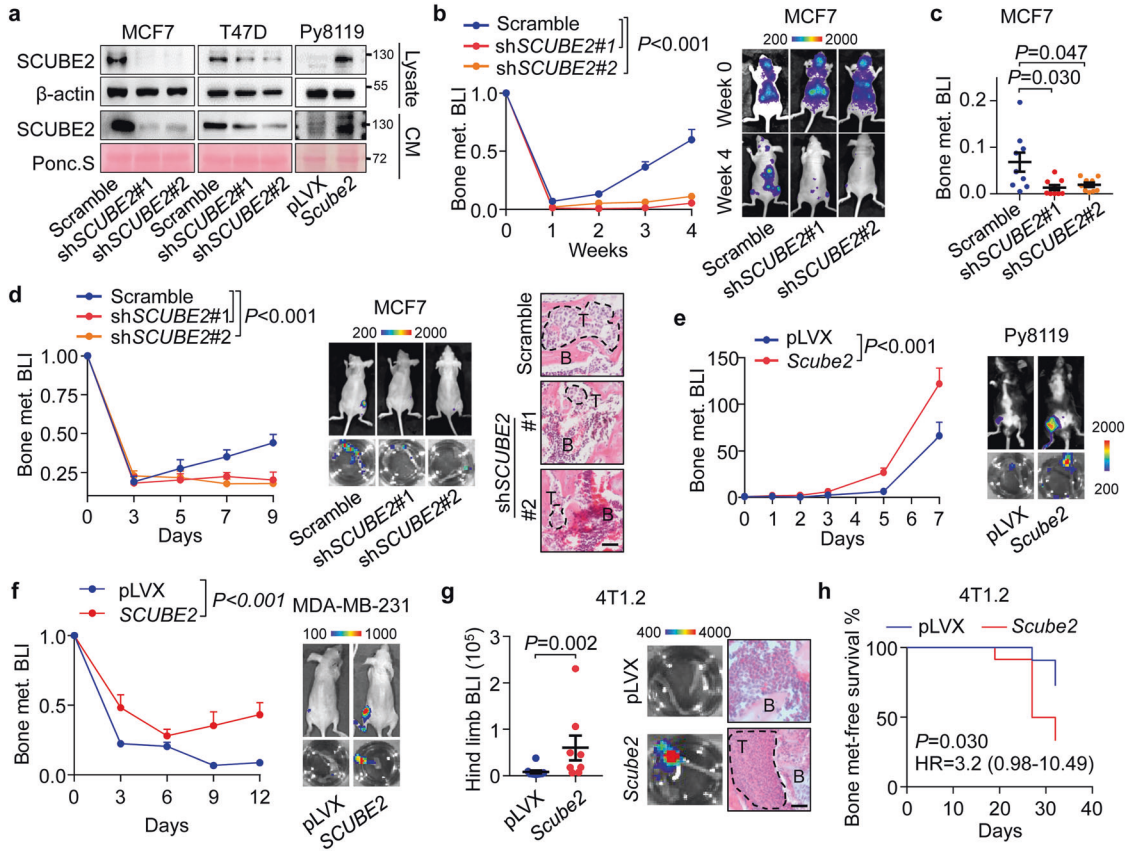

Fig. 2 SCUBE2 promotes bone metastasis of breast cancer. a Validation of *SCUBE2* overexpression and knockdown in different breast cancer cell lines. **b** BLI analyses of bone metastasis by intracardiac injection of MCF7 cells with or without *SCUBE2* knockdown in nude mice ($n = 9$ mice for each group). BLI fold changes normalized to day 0 are shown. **c** Normalized BLI quantification of bone metastasis signals at week 1 in mice of **b**. **d** BLI and hematoxylin & eosin staining (H&E) analyses of early bone colonization after IIA injection of MCF7 cells with or without *SCUBE2* knockdown in nude mice ($n = 6$ mice per group). B bone; T tumor; dotted lines indicate tumor micro-lesion. **e** Normalized BLI quantification after IIA injection of Py8119 cells with or without *Scube2* overexpression in C57 mice ($n = 8$ and 11 mice for control and *Scube2* groups, respectively). **f** Normalized BLI quantification after IIA injection of MDA-MB-231 cells with or without *SCUBE2* overexpression in nude mice ($n = 8$ mice per group). **g**, **h** Orthotopic injection of 4T1.2 cells with or without *Scube2* overexpression in BALB/c mice ($n = 11$ mice per group) for bone metastasis analyses. Shown are ex vivo BLI quantification of hind limbs, representative BLI and H&E staining of bone sections (**g**, dotted lines indicate tumor foci) and bone metastasis-free survival (**h**). *P* values were calculated by two-tailed unpaired *t*-test (**c**, **h**), repeated measures two-way ANOVA (**b**, **d**–**f**) and log-rank test (**h**). Scale bars, 100 μm. Data represent mean ± SEM (**c**, **g**).

To validate relevance of SCUBE2 expression with subtypes and metastasis, we analyzed the mRNA (Supplementary information, Fig. S1e) and protein levels (Fig. 1f) of SCUBE2 in a number of breast cancer cell lines and confirmed the upregulation of SCUBE2 in ER$^+$ luminal cells. Further, we analyzed a Qilu cohort of human breast tumors and found that *SCUBE2* was specifically expressed in luminal tumors (Supplementary information, Fig. S1f) and linked to shortened bone metastasis-free survival in all subtypes (Fig. 1g), as well as in the luminal subtype (Supplementary information, Fig. S1g). We also analyzed the expression of secreted SCUBE2 protein in the blood of patients in Qilu cohort and again observed the upregulation of SCUBE2 in patients with bone recurrence compared to those without distant recurrence (Fig. 1h). Thus, SCUBE2 is highly expressed in luminal breast cancer and positively correlates with bone metastasis.

SCUBE2 is regulated by ER signaling in luminal breast cancer

We investigated the mechanism for SCUBE2 upregulation in luminal tumors. In both the Qilu and Erasmus/MSK cohorts, we observed positive correlations of SCUBE2 expression and secretion with ER status (Fig. 1i; Supplementary information, Fig. S1h, i). In another published clinical dataset GSE3744,[51] *SCUBE2* transcription was also elevated in ER$^+$ tumors (Supplementary information, Fig. S1j), with a strong correlation with expression of estrogen receptor alpha (ERα)-encoding gene *ESR1* (Fig. 1j). To assess whether SCUBE2 is regulated by ER signaling, a number of ER$^+$ breast cancer cells MCF7, BT474, T47D and ZR75-1 were treated with estrogen and significant upregulation of *SCUBE2* expression (Supplementary information, Fig. S1k, l) was observed in all these lines. Treatment with the ER antagonist fulvestrant or tamoxifen significantly inhibited *SCUBE2* expression (Supplementary information, Fig. S1m). Sequence analysis of the *SCUBE2* promoter revealed many potential ERα binding sites. In T47D cells, both *ESR1* overexpression and estrogen significantly enhanced the activity of *SCUBE2* promoter and dual treatment maximized the promoter activation (Fig. 1k). These data suggested that SCUBE2 expression is upregulated by ER signaling in luminal breast cancer.

SCUBE2 promotes bone metastasis of breast cancer

To explore the functional role of SCUBE2 in bone metastasis, *SCUBE2* was stably knocked down in two ER$^+$ luminal cell lines MCF7 and T47D (Fig. 2a; Supplementary information, Fig. S2a). *SCUBE2* knockdown significantly reduced bone metastasis burden following intracardiac injection of cancer cells into mice (Fig. 2b). Noticeably, bioluminescent imaging (BLI) quantification showed that metastasis signal was already prominently suppressed by *SCUBE2* knockdown at the first week after cancer cell inoculation (Fig. 2c), indicating a role of SCUBE2 in the early stage of

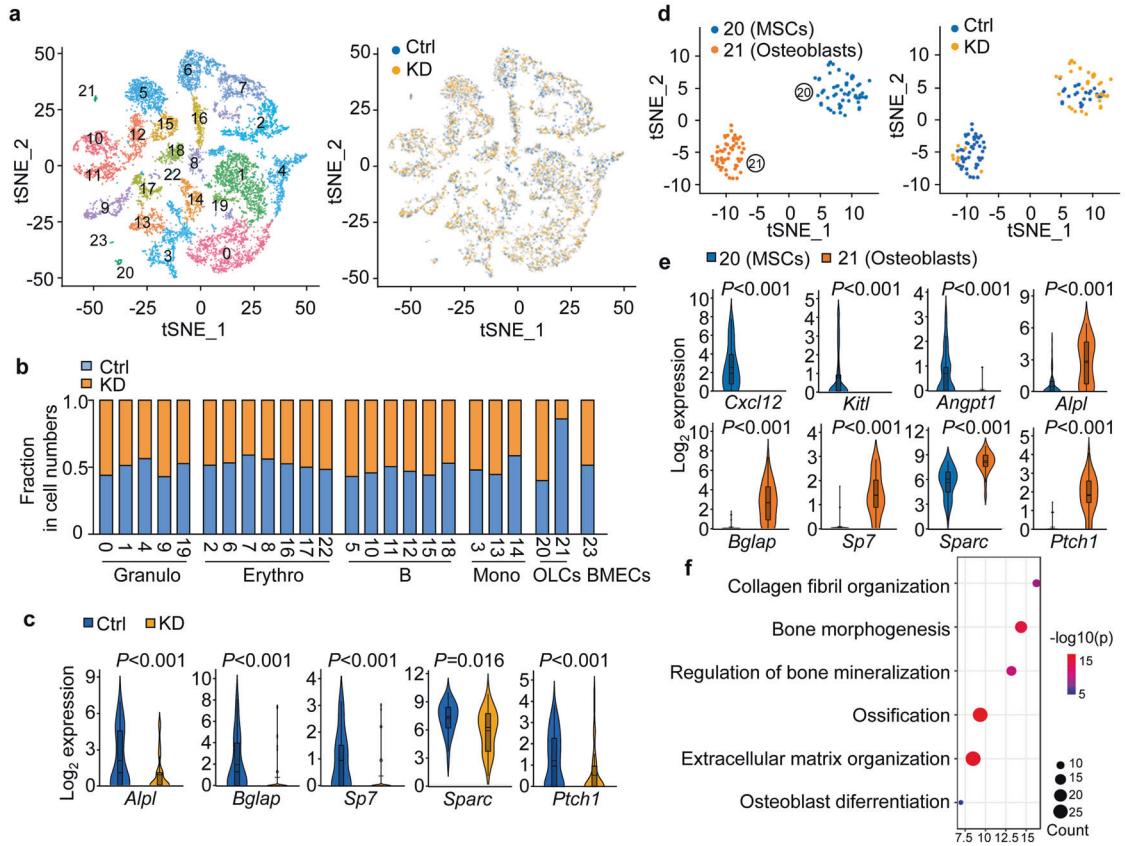

Fig. 3 scRNA-seq analysis identified osteoblast enrichment in bone niches of SCUBE2-expressing tumor cells. a tSNE plots of 18,230 cells in mouse bone niches one week after IIA injection of control (Ctrl) MCF7 cells or those with *SCUBE2* knockdown (KD) ($n = 7$ mice). Cells were grouped into 24 distinct clusters (C0–23), with C1, 4, 9, 19 as granulocytes, C2, 6, 7, 8, 16, 17, 22 as erythrocytes, C3, 13, 14 as monocytes, C5, 10, 11, 12, 15, 18 as B cells, C20, 21 as OLCs, and C23 as BMECs. **b** Relative fraction of cell numbers of each cluster in Ctrl and KD niches. **c** Expression of selected genes in OLCs of Ctrl and KD niches. **d** tSNE plots of OLCs in Ctrl and KD niches. **e** Expression of selected marker genes in the two OLC clusters. **f** GO analysis of enriched genes in C21 vs C20 OLCs.

metastatic colonization. Then we used intra-iliac artery (IIA) injection, an approach selectively delivering cancer cells to hind limbs through the external iliac artery, to monitor early-stage bone colonization.[29] Indeed, *SCUBE2* knockdown in both luminal cell lines reduced cancer cell signal in the hind limbs at early time points after inoculation, resulting in fewer micro-lesions in the bone (Fig. 2d; Supplementary information, Fig. S2b). We further overexpressed *Scube2* in a murine cancer cell line Py8119 derived from the PyMT spontaneous breast tumor (Fig. 2a; Supplementary information, Fig. S2a). Py8119 cells are ER positive, in which *Scube2* expression is responsive to estrogen treatment (Supplementary information, Fig. S2c). *Scube2* overexpression did not affect mammary tumor growth of Py8119 cells (Supplementary information, Fig. S2d), but resulted in increased bone metastasis in immunocompetent mice following IIA injection of the cells (Fig. 2e), further confirming the role of SCUBE2 in bone metastasis of luminal cancer.

Although *SCUBE2* is upregulated in luminal breast cancer, its effect on metastasis may or may not be luminal subtype-dependent. To investigate this, we stably overexpressed *SCUBE2* in a triple-negative breast cancer cell line MDA-MB-231 (Supplementary information, Fig. S2e, f), and still observed a significant exacerbation of bone colonization in a week after IIA inoculation of the cells into nude mice (Fig. 2f), indicating that the pro-metastasis effect of SCUBE2 may not rely on luminal cell context once it is upregulated. We further orthotopically implanted the murine 4T1.2 breast cancer cells[52] with *Scube2* overexpression (Supplementary information, Fig. S2e, f) into the mammary fat pads of BALB/c mice to assess the effect of *Scube2* in spontaneous metastasis model. SCUBE2 had no effect on primary tumor growth (Supplementary information, Fig. S2g), but prominently accelerated bone metastasis in the hind limbs (Fig. 2g) and shortened bone metastasis-free survival (Fig. 2h). These findings demonstrated a pro-bone metastatic role of SCUBE2 during the early colonization stage.

Since SCUBE2 influenced bone colonization without affecting primary tumor growth, we further analyzed its effects on in vitro cancer cell growth, invasion, migration and apoptosis, and observed that *SCUBE2* overexpression or knockdown did not obviously regulate these intrinsic properties of cancer cells (Supplementary information, Fig. S2h–k), suggesting a microenvironment-dependent role of SCUBE2 in bone metastasis.

SCUBE2 promotes osteoblast differentiation in bone metastasis niches

Thus, single-cell RNA sequencing (scRNA-seq) analysis was performed to explore the cellular components in bone metastasis niches one week after IIA injection of MCF7 cells into BALB/c nude mice. $CD45^-$ stromal cells were enriched for the analysis, since the majority of bone marrow cells are $CD45^+$ immune cells (Supplementary information, Fig. S3a). Unbiased clustering of the scRNA-seq data revealed 24 cell clusters of 6 major groups, in the metastasis niches (Fig. 3a; Supplementary information, Fig. S3b–e), including granulocytes expressing *Cebpe*[53] (clusters 0, 1, 4, 9 and 19), erythrocytes expressing *Hba-a2*[54] (clusters 2, 6, 7, 8, 16, 17 and 22), B cells expressing *Cd19*[55] (clusters 5, 10, 11, 12, 15 and 18), monocytes expressing *Csf1r*[56] (clusters 3, 13 and 14), osteolineage cells (OLCs) expressing *Alpl*[57] (clusters 20 and 21) and

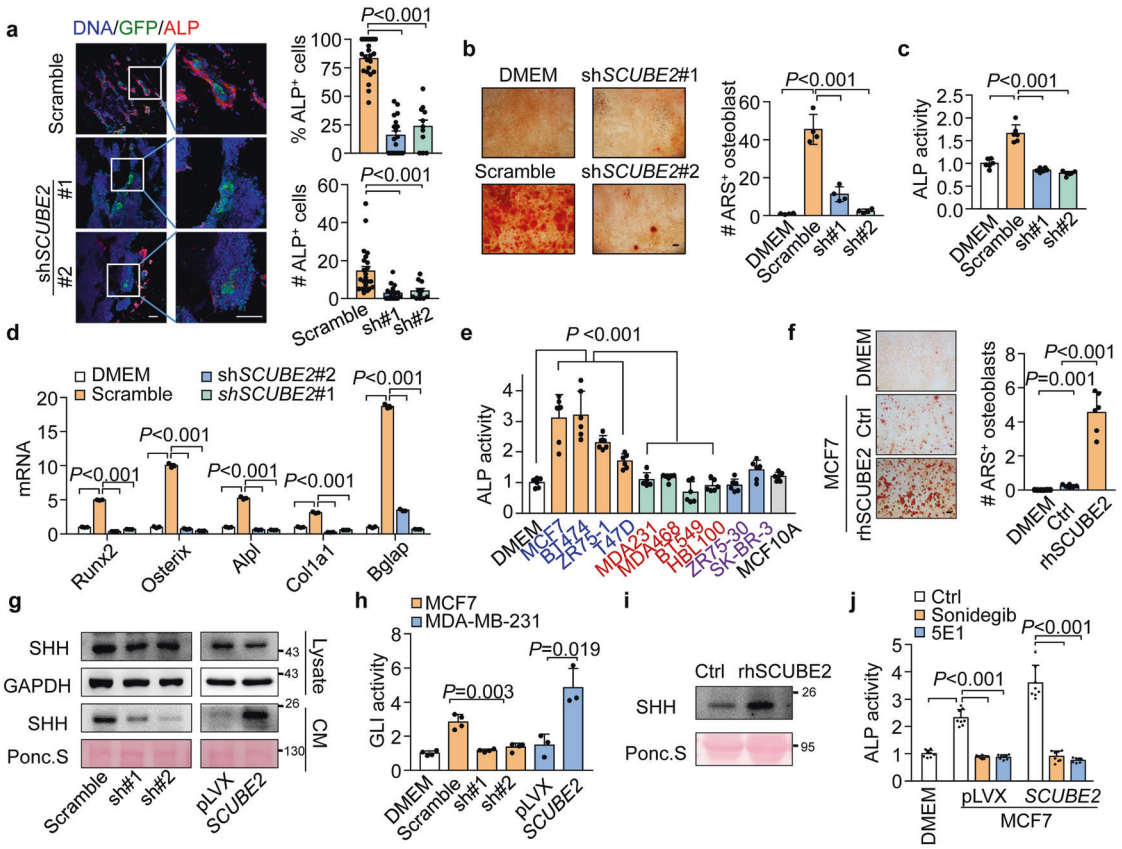

Fig. 4 SCUBE2 promotes osteogenic niche formation by releasing tumoral SHH. a IF analyses of ALP$^+$ osteoblasts around GFP$^+$ cancer cells in bones at day 7 after IIA injection of MCF7 cells with or without *SCUBE2* knockdown. The numbers and percentages of ALP$^+$ osteoblasts in stromal cells in direct contact with microscopic lesions are shown ($n = 23$, 18 and 11 random microscopic fields (RMFs) from 4 mice per group). **b**–**d** Osteoblast differentiation of MSCs induced by control DMEM medium or CM from MCF7 cells with or without *SCUBE2* knockdown. Shown are Alizarin Red S (ARS) staining (**b**), ALP activity (**c**), and mRNA levels of osteoblastogenesis marker genes (**d**). **e** ALP activity of MSCs treated with CM of luminal (blue), TN (red), HER2$^+$ (purple) cancer and normal (black) mammary cell lines. **f** ARS staining of MSC-derived osteoblasts induced by DMEM or CM from rhSCUBE2-treated MCF7 cells. **g** SHH expression and release after *SCUBE2* knockdown or overexpression in MCF7 cells. **h** GLI reporter activity in MC3T3 cells treated with DMEM, or CM of MCF7 cells with or without *SCUBE2* knockdown, or CM of MDA-MB-231 cells with or without *SCUBE2* overexpression. **i** SHH secretion by rhSCUBE2-treated MCF7 cells. **j** ALP activity of MSC-derived osteoblasts with treatment of CM from MCF7 cells with or without *SCUBE2* overexpression, and/or Sonidegib or 5E1. *P* values were calculated by two-tailed unpaired *t*-test. Scale bars, 100 μm. Data represent mean ± SEM (**a**) or mean ± SD (others). $n = 4$ (**b**, **h**, **j**) or 6 (**c**, **f**) biologically independent samples.

bone marrow endothelial cells (BMECs) expressing *Cdh5*[58] (cluster 23). We compared the niche composition of MCF7 cells with or without *SCUBE2* knockdown, and found that the fraction of OLCs displayed the most obvious change (Supplementary information, Fig. S3f). Analyses of all the cell clusters also showed that cluster 21 of OLCs was dramatically depleted by *SCUBE2* knockdown, but the changes of other clusters were not manifest (Fig. 3a, b). Osteogenic genes, such as *Alpl*, *Bglap*, *Sp7*, and pathways, such as ossification and collagen formation, were downregulated in OLCs after *SCUBE2* knockdown (Fig. 3c; Supplementary information, Fig. S3g), indicating the regulation of osteoblastic function by *SCUBE2*. Although SCUBE2 was previously reported to function as a VEGFR2 co-receptor and regulate angiogenesis,[59] we did not observe obvious changes either in the abundance or CD31 activity of endothelial cells in the bone after *SCUBE2* knockdown (Supplementary information, Fig. S3f, h, i).

Further analysis of OLCs confirmed the depletion of cluster 21, but not cluster 20, after *SCUBE2* knockdown (Fig. 3d). Cluster 20 was annotated as mesenchymal stromal cells (MSCs) and cluster 21 as osteoblasts according to previously identified markers of these two cell types[60,61] (Fig. 3e). GO analysis also validated the enrichment of osteoblast-specific pathways in cluster 21 as compared to cluster 20 (Fig. 3f). Collectively, scRNA analysis revealed a depletion of osteoblasts in the bone metastasis niches after *SCUBE2* knockdown in cancer cells.

Validating the scRNA-seq analyses, both immunohistochemistry and immunofluorescent (IF) staining demonstrated the decreased number and percentage of alkaline phosphatase (ALP)$^+$ osteoblasts surrounding *SCUBE2*-deficient tumor cells, while *SCUBE2* overexpression in human and murine breast tumor cells led to the enrichment of osteoblasts in early bone niches (Fig. 4a; Supplementary information, Fig. S4a, b). In contrast, the abundance of osteoclasts, which are often induced during the outgrowth stage of breast cancer bone colonization, was not obviously changed in the early metastatic niches (Supplementary information, Fig. S4a).

Consistent with the analyses of metastasis sections of the mice, in vitro assays confirmed the role of SCUBE2 in differentiation of osteoblasts (Fig. 4b–d), but not osteoclasts (Supplementary information, Fig. S4c). *SCUBE2* knockdown significantly inhibited the ability of tumor cell conditioned medium (CM) to induce osteogenic differentiation from MSCs, leading to less mineralization, declined ALP activity and suppressed expression of osteoblastogenesis-related genes (Fig. 4b–d). Consistently, SCUBE2 upregulation in multiple breast cancer cell lines markedly enhanced the ability of their CM to induce MSC differentiation into osteoblasts (Supplementary information, Fig. S4d, e). Fulvestrant

treatment of MCF7 cells significantly inhibited CM-induced osteoblast differentiation (Supplementary information, Fig. S4f, g). Furthermore, CM of luminal breast cancer cells, which express higher levels of SCUBE2 (Fig. 1f), showed stronger osteoblast-inducing abilities than cell lines of other subtypes (Fig. 4e). These data confirmed that SCUBE2 enhances osteogenic maturation.

SCUBE2 induces osteogenic differentiation by mediating SHH release from tumor cells

To investigate how tumoral SCUBE2 influences osteoblast differentiation, the recombinant human SCUBE2 (rhSCUBE2) protein was used in osteoblast differentiation culture. Direct treatment of MSCs with rhSCUBE2 had no impact on osteoblast maturation (Supplementary information, Fig. S4h), while rhSCUBE2 treatment of tumor cells significantly increased the ability of tumoral CM to induce osteoblast differentiation from MSCs (Fig. 4f; Supplementary information, Fig. S4i). These data suggested that tumor-secreted SCUBE2 plays an autocrine role to regulate osteoblasts. Previous studies reported that SCUBE2 promotes SHH release into the extracellular space and enhances SHH activity in some cell types.[35,36,38] Concordantly, our data showed that *SCUBE2* expression resulted in enhanced secretion, but not expression, of SHH in cancer cells (Fig. 4g; Supplementary information, Fig. S4j). In addition, MCF7 CM could activate the Hedgehog signaling in MC3T3 cells transfected with a GLI-dependent luciferase reporter, while *SCUBE2* knockdown in MCF7 cells attenuated Hedgehog signaling activation in MC3T3 cells (Fig. 4h). In contrast, *SCUBE2* overexpression in MDA-MB-231 cells enhanced tumoral CM-induced Hedgehog signaling activation in MC3T3 cells (Fig. 4h). This was consistent with the scRNA-seq data showing the downregulation of Hedgehog downstream gene *Ptch1* in osteoblasts after *SCUBE2* knockdown (Fig. 3c, e).

In addition, treating MCF7 cells with rhSCUBE2 protein led to a higher extracellular SHH level (Fig. 4i). Direct treatment of MSCs with recombinant human SHH protein accelerated osteoblast differentiation (Supplementary information, Fig. S4k). Inhibiting SHH in MCF7 CM with an SHH-neutralizing antibody 5E1 or the Hedgehog signaling inhibitor Sonidegib significantly suppressed CM-induced osteogenic differentiation of MSCs (Fig. 4j). More importantly, both 5E1 and Sonidegib could completely block the effect of *SCUBE2* overexpression on osteoblastogenesis, resulting in decreased ALP activity (Fig. 4j) and expression of osteogenic markers in osteoblasts (Supplementary information, Fig. S4l). In addition, analysis of the bone metastases from MCF7 cells demonstrated the expression of SHH mainly by tumor cells (Supplementary information, Fig. S4m). Clinically, breast tumors with high expression of both *SCUBE2* and *SHH* displayed exacerbated bone metastasis (Supplementary information, Fig. S4n). Together, these data indicated that SCUBE2 plays its role by enhancing tumoral SHH secretion.

SCUBE2 promotes bone metastasis by activating Hedgehog signaling in pre-osteoblasts

To further interrogate whether Hedgehog signaling activation in osteoblasts mediates the pro-metastatic effect of tumoral SCUBE2, Hedgehog signaling in MSCs was constitutively suppressed by *Smo* knockdown (Fig. 5a; Supplementary information, Fig. S5a) or activated by *Gli1* overexpression (Supplementary information, Fig. S5b, c). *Smo* inhibition resulted in reduction of osteoblast maturation (Fig. 5b), ALP activity (Fig. 5c) and osteogenic gene expression (Fig. 5d), while *Gli1* overexpression significantly promoted osteoblast differentiation (Supplementary information, Fig. S5d–f). These data were concordant with previous reports[62,63] that Hedgehog signaling plays a positive role in osteogenic differentiation. Importantly, Hedgehog inhibition in MSCs completely diminished the pro-osteogenic effect of SCUBE2 (Fig. 5e, f). To explore the function of Hedgehog signaling in bone metastasis, Py8119 cancer cells with *Scube2* overexpression and MSCs with *Smo* knockdown were co-administered into mice by IIA injection. Notably, Hedgehog inhibition in MSCs totally blocked the effect of SCUBE2 in tumor cells for bone metastasis, resulting in decrease of osteoblasts in the early niches and delayed metastasis (Fig. 5g; Supplementary information, Fig. S5g, h). Concordantly, MSCs and osteoblasts, including MC3T3 and hFOB1.19 cells, all expressed high levels of Hedgehog receptors and signaling component proteins, including SMO, PTCH1, PTCH2 and GLI1. The expression of Hedgehog components was further elevated in MSCs when differentiated into osteoblasts (Supplementary information, Fig. S5i). In contrast, their expression was much lower in breast cancer cells (Supplementary information, Fig. S5i). Hedgehog signaling inhibition in *Scube2*-overexpressing cancer cells by *Smo* knockdown (Supplementary information, Fig. S5j) had no impact on in vivo bone metastasis (Supplementary information, Fig. S5k).

However, when *SHH* expression was silenced in MCF7 cells with *SCUBE2* overexpression (Fig. 5h), the pro-osteogenic ability of MCF7 CM and in vivo bone metastasis from MCF7 cells were markedly suppressed. Importantly, the effects of *SCUBE2* overexpression were completely blocked (Fig. 5i, j). Collectively, these data showed that SCUBE2 promotes bone metastasis by facilitating tumoral SHH secretion, leading to Hedgehog signaling activation and osteogenic differentiation of pre-osteoblasts.

Osteogenic niches protect tumor cells from immune cytotoxicity

Next, we explored how SCUBE2-induced osteogenic niches affect bone colonization of breast cancer. It was observed that *SCUBE2* knockdown did not affect the proliferation (Supplementary information, Fig. S6a), but significantly promoted the apoptosis (Supplementary information, Fig. S6b) of cancer cells in bone. Concordantly, *Scube2* overexpression reduced the percentage of cleaved Caspase3$^+$ apoptotic tumor cells (Fig. 6a). This was in contrast with our previous data showing that SCUBE2 had no effect on apoptosis of tumor cells in vitro (Supplementary information, Fig. S2k), indicating the involvement of osteoblasts or other microenvironmental components in regulation of tumor cell apoptosis.

Notably, we also observed the enhanced presence of NKp46$^+$ natural killer (NK) cells in the osteoblast-deprived niches surrounding *SCUBE2*-deficient tumor cells in IF analyses, while NK cells were depleted by *Scube2* overexpression, revealing a negative correlation between osteoblasts and NK cell activation in the niches (Fig. 6b; Supplementary information, Fig. S6c). Thus, we analyzed the CD45$^+$ immune cells in early bone metastasis niches from MCF7 cells with or without *SCUBE2* knockdown by scRNA-seq (Supplementary information, Fig. S6d), which revealed 15 cell clusters (Supplementary information, Fig. S6e–g). The expression of genes and pathways related to immune activation was significantly elevated in NK cells (cluster 13) after *SCUBE2* knockdown (Fig. 6c; Supplementary information, Fig. S6h, i). Flow cytometry (FACS) analysis of niche cells also confirmed these observations (Fig. 6d; Supplementary information, Fig. S6j). In addition, SCUBE2 promoted bone metastasis in nude mice (Fig. 2b), but not in severely immunodeficient NSG mice (Supplementary information, Fig. S6k), further suggesting a role of NK cells in SCUBE2-mediated regulation of bone metastasis.

Then we tested whether osteoblasts and NK cells are involved in regulation of tumor apoptosis with in vitro immune killing assays (Supplementary information, Fig. S7a). Co-culturing MCF7 cells with NK92 NK cells caused obvious tumor cell apoptosis, but supplementing hFOB1.19 osteoblasts in the co-culture reduced apoptosis of MCF7 cells. The tumor-protective effect of hFOB1.19 cells was significantly higher than that of undifferentiated MSCs (Supplementary information, Fig. S7b). Osteoblasts also protected the patient-derived organoids (PDOs) of luminal breast cancer from NK killing (Fig. 6e, f). The CM of osteoblasts showed similar protective effects (Supplementary information,

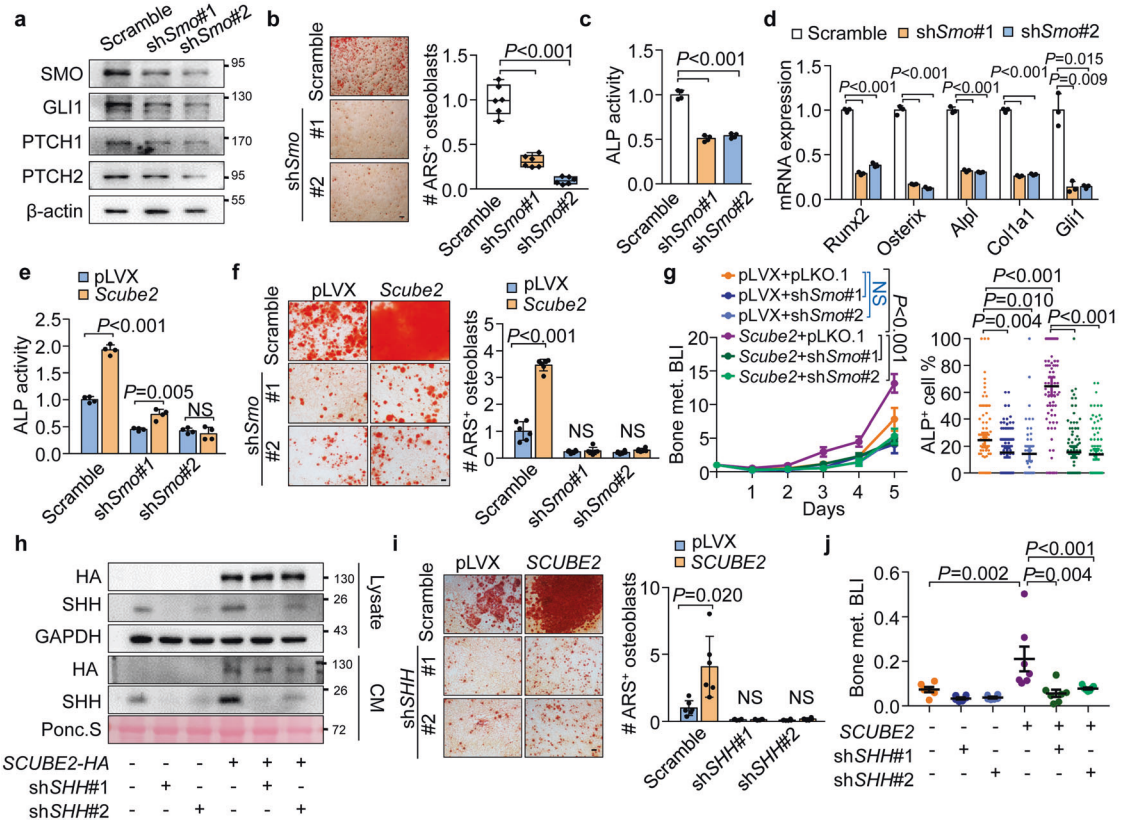

Fig. 5 SCUBE2 promotes bone metastasis by activating Hedgehog signaling in pre-osteoblasts. a Expression of Hedgehog signaling components in MSCs after *Smo* knockdown. **b**–**d** ARS staining (**b**), ALP activity (**c**) and expression of osteoblastogenesis marker genes (**d**) in osteoblasts derived from MSCs with or without *Smo* knockdown. **e**, **f** ALP activity (**e**) and ARS staining (**f**) of osteoblasts derived from MSCs with *Smo* knockdown and/or treatment of CM from Py8119 cells with or without *Scube2* overexpression. **g** IIA injection of mixed Py8119 cells (with or without *Scube2* overexpression) and MSCs (with or without *Smo* knockdown) into C57 mice ($n = 5$ mice per group). Shown are BLI of bone metastasis (left) and IF analyses of ALP^+ osteoblast percentages around GFP^+ cancer cells in bone sections (right, $n = 86$–93 RMFs from 4 mice per group). **h** SHH expression and secretion in MCF7 cells with *SCUBE2* overexpression and/or *SHH* knockdown. **i** ARS staining of MSC-derived osteoblasts treated with CM from MCF7 cells with *SCUBE2* overexpression and/or *SHH* knockdown. **j** Bone metastasis of MCF7 cells with *SCUBE2* overexpression and/or *SHH* knockdown after IIA injection in nude mice ($n = 6$–7 mice per group). Scale bars, 100 μm. *P* values were calculated by two-tailed unpaired *t*-test (**b**–**g**, **i**, **j**) and repeated measures two-way ANOVA (**g**). NS not significant. Data represent mean ± SD (**c**–**f**, **i**) or mean ± SEM (**g**, **j**). Box plots display values of the minimum, first quartile, median, third quartile and maximum (**b**). $n = 4$ (**b**, **e**) or 6 (**c**, **f**, **i**) biologically independent samples.

Fig. S7c). Pre-treating MSCs with SCUBE2-expressing tumor cell CM to enhance osteoblast differentiation would further promote tumor protection, while *SCUBE2* knockdown or fulvestrant treatment of tumor cells abrogated such an effect (Fig. 6g; Supplementary information, Fig. S7d). However, SCUBE2 had no impact on NK92 cytotoxicity of tumor cells in the absence of osteoblasts (Supplementary information, Fig. S7e). Concordantly, osteoblasts treated with tumor cell CM or *Gli* overexpression inhibited the expression of cytotoxic cytokines, including IFNγ and TNFα, in NK92 cells, as shown by both mRNA and FACS analyses (Fig. 6h, i; Supplementary information, Fig. S7f), leading to enhanced tumor protection (Supplementary information, Fig. S7g). These data suggested that certain extracellular factors expressed by differentiated osteoblasts suppress lymphocyte activation and protect tumor cells from immune cytotoxicity.

Osteoblasts inhibits NK cells via collagen-LAIR1 signaling

To examine how osteoblasts suppress lymphocytes, we compared the expression profiles of MSCs and MSC-derived osteoblasts which were treated with CM of MCF7 cells with or without *SCUBE2* knockdown by mRNA sequencing. Gene set enrichment analysis (GSEA) and GO analyses showed the upregulation of molecular pathways related to immune regulation, Hedgehog signaling and osteoblast differentiation[64,65] in MSCs treated with *SCUBE2*-expressing tumor CM (Fig. 7a, b; Supplementary information, Fig. S8a), corroborating the effects of SCUBE2 on osteoblasts. Interestingly, several collagen and extracellular matrix (ECM)-related signatures were also upregulated in SCUBE2-induced osteoblasts (Fig. 7a, b). Indeed, many collagen-encoding genes were upregulated in MSCs by tumor CM, and the upregulation was dependent on *SCUBE2* expression in cancer cells (Fig. 7c). This was consistent with the scRNA-seq analysis showing the upregulation of collagen-related pathways in OLCs enhanced by SCUBE2 (Fig. 3f; Supplementary information, Fig. S3g).

Collagens are major components of ECM and are known to play crucial roles in tumor progression and metastasis.[66–68] More recently, it was found that collagens act as ligands of the inhibitory receptor LAIR1 of immune cells,[69–71] which suppresses lymphocytic activity through SHP1 signaling.[72–74] Among the collagen superfamily, collagen type 1 (COL1) is the major organic component of bone[75] and expressed mainly by osteoblasts.[76] COL1 expression and secretion in MSC-derived osteoblasts were enhanced by *SCUBE2*-expressing tumor CM or Hedgehog signaling activation in MSCs (Supplementary information, Fig. S8b). More importantly, IF staining of bone sections revealed reduced COL1 level around tumor cells with *SCUBE2* knockdown (Supplementary information, Fig. S8c), while *Scube2* overexpression enhanced COL1 expression in the niches (Supplementary information,

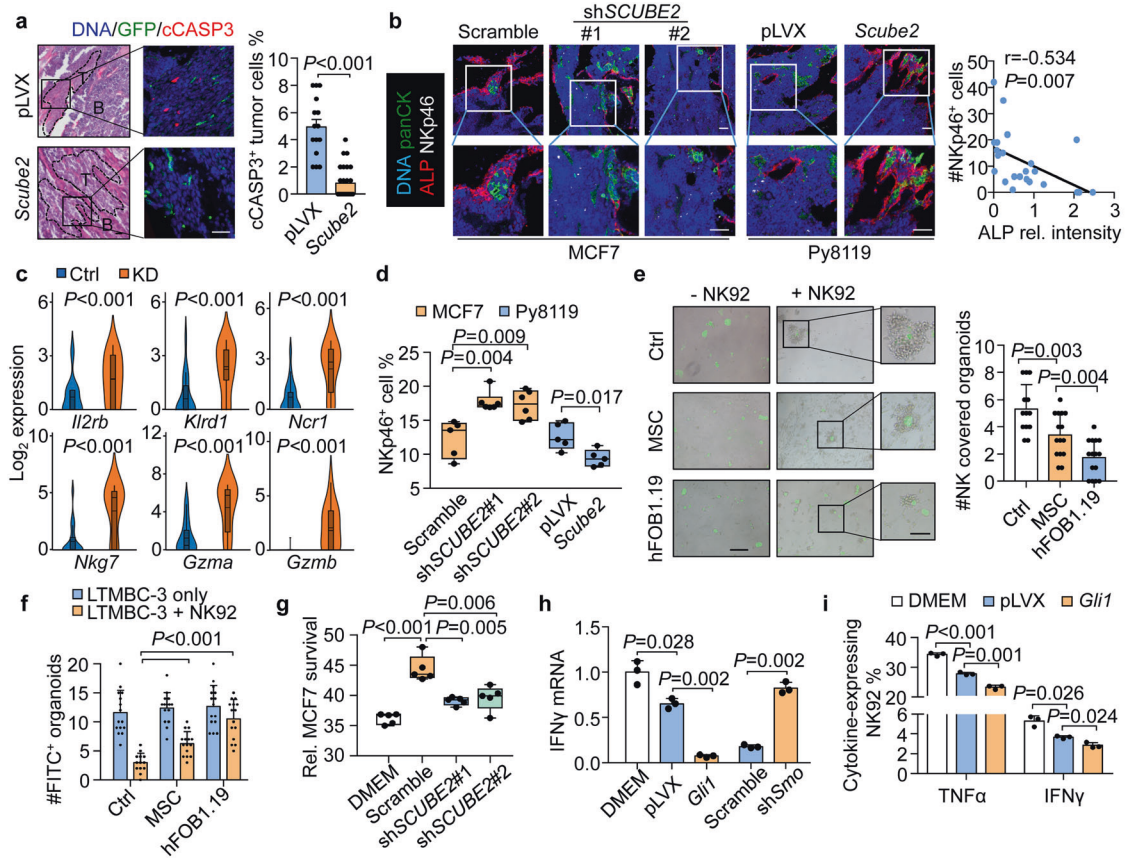

Fig. 6 Osteoblasts promote tumor survival by immune suppression. a IF analyses of cleaved Caspase3 (cCASP3) for tumor apoptosis in bone at day 5 after IIA injection of GFP$^+$ Py8119 cells with or without *Scube2* overexpression ($n = 15$ and 27 RMFs from 3 mice per group). **b** IF analyses of ALP$^+$ osteoblasts and NKp46$^+$ NK cells in bone niches at day 7 after IIA injection of MCF7 cells (with or without *SCUBE2* knockdown) or Py8119 cells (with or without *Scube2* overexpression). Shown are representative images and correlation of ALP intensity with number of NK cells in MCF7 niches. **c** Expression of selected genes measured by scRNA-seq in NK cells of control (Ctrl) and *SCUBE2*-deficient (KD) MCF7 niches. **d** FACS analyses of NK cells in bone niches at day 7 after IIA injection of MCF7 cells (with or without *SCUBE2* knockdown) or Py8119 cells (with or without *Scube2* overexpression). **e**, **f** Analyses of immune killing of a luminal PDO sample LTMBC-3 co-cultured with NK92 cells and the indicated cells for 48 h. LTMBC-3 was pre-labeled with FITC. Shown are representative images of organoids, numbers of NK92-covered organoids (**e**) and numbers of surviving organoids (**f**, $n = 4$ biologically independent samples). **g** In vitro immune killing of MCF7 cells by NK92 cells, after treatment with DMEM or CM from MSC-derived osteoblasts which were pre-treated with CM from MCF7 cells with or without *SCUBE2* knockdown ($n = 6$ biologically independent samples). See assay setup in Supplementary information, Fig. S6j. **h**, **i** *IFNγ* mRNA expression (**h**) and FACS analyses of TNFα and IFNγ protein expression (**i**) in NK92 cells after treatment with CM from MSC-derived osteoblasts with *Gli1* overexpression or *Smo* knockdown for 24 h. *P* values were calculated by two-tailed unpaired *t*-test. Scale bars, 100 μm. Data represent mean ± SEM (**a**) or mean ± SD (others). Box plots display values of the minimum, first quartile, median, third quartile and maximum (**d**, **g**).

Fig. S8d). Furthermore, recombinant COL1 protein was able to dose-dependently protect MCF7 cells from immune killing of NK92 cells in lymphocyte–tumor co-culture (Fig. 7d), and rescue immune suppression which was downregulated by *Smo* knockdown of osteoblasts in lymphocyte–osteoblast–tumor co-culture (Supplementary information, Fig. S8e). Knockdown of the collagen receptor *LAIR1* in NK92 cells (Supplementary information, Fig. S8f) efficiently relieved osteoblast-mediated immune suppression (Fig. 7e). Treating the co-culture with LAIR2, a soluble LAIR1 competitive ligand antagonizing collagen–LAIR1 interaction,[26] also dose-dependently reduced the immune-suppressive effect of osteoblast CM (Fig. 7f). In addition, an elevation of SHP1 phosphorylation, along with the suppression of lymphocytic cytokines downstream of LAIR1, was observed in NK92 cells when the lymphocytes were treated with CM from Hedgehog signaling-activated osteoblasts, while Hedgehog signaling inhibition in osteoblasts or *SCUBE2* knockdown in tumor cells led to the opposite effects (Fig. 7g–i).

Since LAIR1 is widely expressed by immune cells,[77,78] we hypothesized that osteoblasts may also regulate other immune cells. Indeed, COL1 protein could also suppress the cytotoxicity of Jurkat T cells (Supplementary information, Fig. S8g). Furthermore, tumoral *SCUBE2* knockdown or osteoblastic *Smo* knockdown relieved T cell suppression, while Hedgehog signaling activation in osteoblasts enforced the suppression, together with regulation of cytotoxic cytokines and LAIR1 downstream cytokines in T cells (Supplementary information, Fig. S8h–l). We also observed a slight decrease of CD8$^+$ T cells and significant depletion of cytotoxic cytokines in the early bone niches of *SCUBE2*-overexpressing tumor cells (Supplementary information, Fig. S8m, n). By contrast, macrophage polarization was not affected by SCUBE2 (Supplementary information, Fig. S8o). Thus, these data revealed a SCUBE2-Hedgehog-collagen axis in early metastatic niches to suppress NK cells and other lymphocytes during luminal breast cancer bone metastasis (Fig. 7j).

SCUBE2 expression correlates with osteoblast differentiation and immune suppression in clinical bone metastases

Next, we assessed the clinical relevance of SCUBE2 expression with osteoblast differentiation and lymphocyte infiltration in human breast cancer. IF staining of clinical bone metastases demonstrated significantly elevated ALP$^+$ osteoblasts and COL1

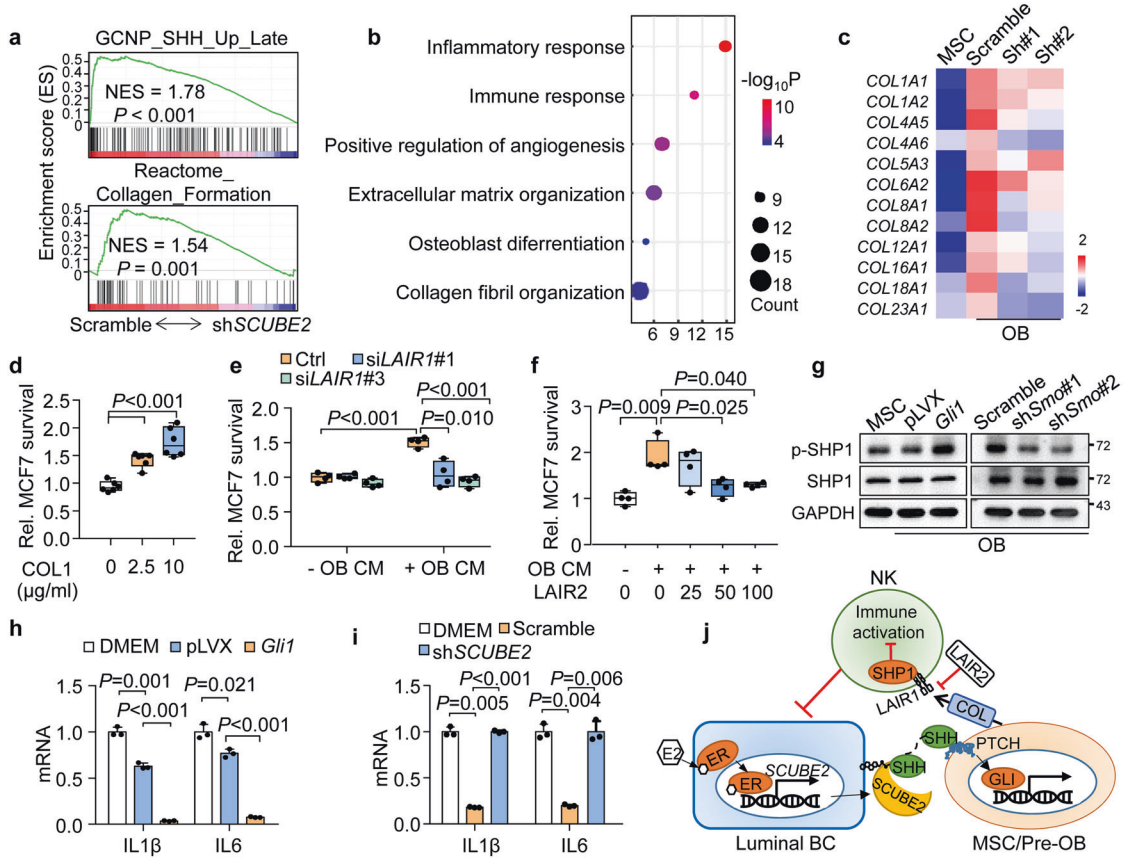

Fig. 7 The collagen-LAIR1 axis mediates osteoblast-induced immune suppression. a, **b** GSEA analyses of SHH-upregulated (top) and collagen formation (bottom) gene sets (**a**) and GO analyses of enriched genes (**b**) in the RNA-seq profiles of MSC-derived osteoblasts treated with CM from control vs *SCUBE2*-deficient MCF7 cells. **c** Expression heatmap of collagen-encoding genes in undifferentiated MSCs or MSC-derived osteoblasts treated with CM from control or *SCUBE2*-deficient MCF7 cells. **d** In vitro immune killing of MCF7 cells by NK92 cells treated with various concentrations of COL1 protein. **e** In vitro immune killing of MCF7 cells by NK92 cells with *LAIR1* knockdown, and/or with osteoblast (OB) CM. **f** In vitro immune killing of MCF7 cells by NK92 cells treated with osteoblast CM and/or various concentrations of LAIR2 protein. **g** SHP1 phosphorylation in NK92 cells treated with CM from undifferentiated MSCs or MSC-derived osteoblasts with *Gli1* overexpression or *Smo* knockdown. **h**, **i** LAIR1 downstream cytokine mRNA expression in NK92 cells cultured in CM from osteoblasts differentiated from MSCs with or without *Gli1* overexpression (**h**) or treated with CM from MCF7 cells with or without *SCUBE2* knockdown (**i**). See assay setup in Supplementary information, Fig. S6j. **j** A schematic model depicting the role of SCUBE2 in bone metastasis of luminal breast cancer (BC). *P* values were calculated by two-tailed unpaired *t*-test (**d**–**f**, **h**, **i**). Data represent mean ± SD (**h**, **i**). Box plots display values of the minimum, first quartile, median, third quartile and maximum (**d**–**f**). $n = 4$ biologically independent samples (**d**–**f**).

deposition around SCUBE2$^+$ tumor cells, forming an osteogenic niche (Fig. 8a; Supplementary information, Fig. S9a), showing obvious positive correlation of tumoral SCUBE2 expression to ALP and COL1 intensities (Fig. 8b; Supplementary information, Fig. S9b). In addition, significantly fewer NKp46$^+$ NK cells and Granzyme B (GZMB)$^+$ lymphocytes were observed in metastases with higher SCUBE2 expression (Fig. 8a; Supplementary information, Fig. S9c, d). Negative correlations were observed between infiltration of NK cells with SCUBE2 expression, and between infiltration of GZMB$^+$ lymphocytes with SCUBE2 and COL1 expression in the metastases (Fig. 8c; Supplementary information, Fig. S9d–f). Besides, SCUBE2 expression was higher in bone metastases of ER$^+$ tumors than those of ER$^-$ tumors (Supplementary information, Fig. S9g). These data corroborated the role of SCUBE2 in bone metastasis of luminal cancer.

Targeting Hedgehog signaling with Sonidegib prevents bone metastasis in mice

Given the critical role of Hedgehog signaling in osteoblastic niche, we tested the effect of Hedgehog signaling targeting on bone metastasis. Sonidegib is a Hedgehog signaling inhibitor and therapeutic candidate for some tumors,[79–82] but its efficacy to treat breast cancer metastasis has not been tested. BALB/c mice with intracardiac implantation of 4T1.2 cells were treated by daily oral administration of Sonidegib. The treatment reduced ALP expression around tumor cells and recovered NK cell infiltration in bone lesions (Supplementary information, Fig. S10a), leading to alleviated bone metastasis burden (Fig. 8d), and extended survival of the mice (Fig. 8e). We further assessed the effects of Sonidegib on spontaneous bone metastasis by orthotopically implanting 4T1.2 cells with *Scube2* overexpression into BALB/c mice. Sonidegib had no effect on primary tumor growth (Supplementary information, Fig. S10b), but significantly inhibited bone metastasis (Fig. 8f). In addition, Sonidegib was also effective to suppress bone metastasis of human MCF7 cells in nude mice (Supplementary information, Fig. S10c).

A SCUBE2 neutralizing antibody effectively suppresses bone metastasis of breast cancer

The specific high expression of SCUBE2 in luminal breast cancer, but not in normal tissues or other breast cancer subtypes (Fig. 1c, f; Supplementary information, Fig. S1c, e), indicates the potential of SCUBE2 as a therapeutic target for luminal breast cancer. Thus, we sought to develop a SCUBE2 neutralizing antibody targeting the CUB domain which is essential for SHH shedding,[40] and successfully identified an IgG monoclone LTMA16D5 by functional

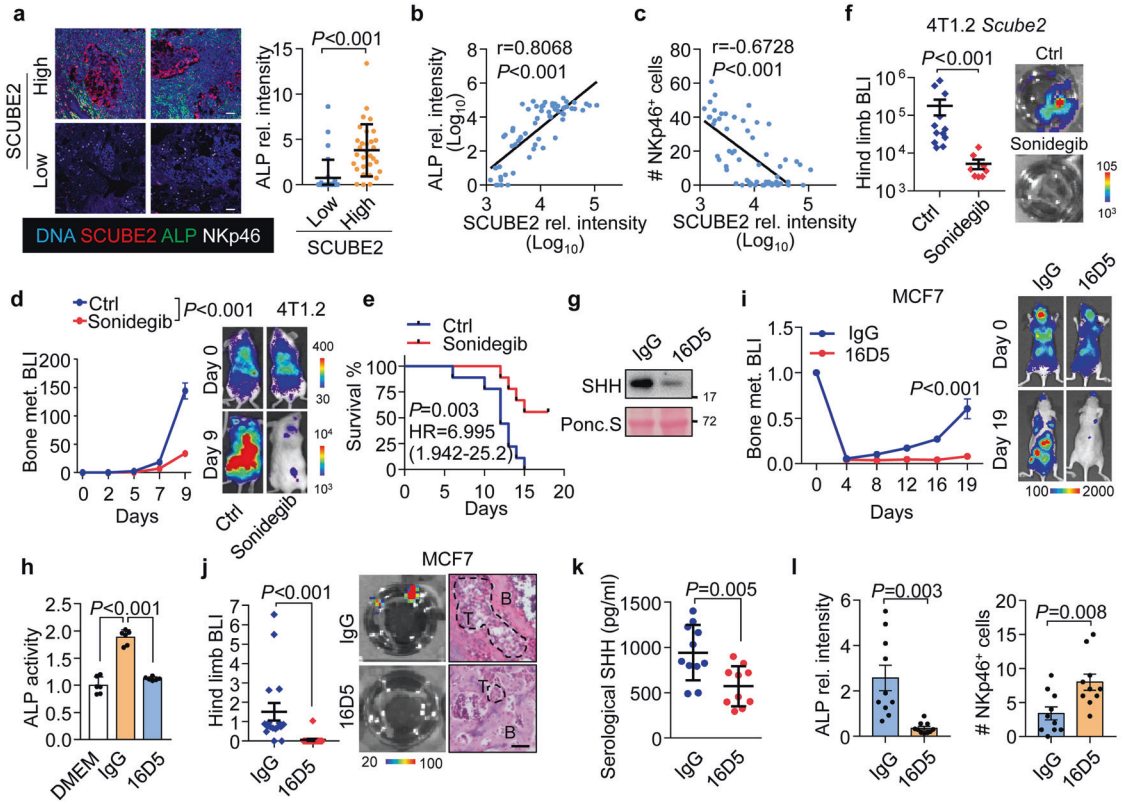

Fig. 8 Clinical relevance and therapeutic targeting of Hedgehog signaling and SCUBE2 in bone metastasis. a–c IF analyses of SCUBE2 expression, osteoblasts (ALP) and NK cells (NKp46) in human bone metastases ($n = 20$) of the Qilu breast cancer cohort. Shown are representative IF images and ALP expression in samples grouped by SCUBE2 expression (**a**), correlation between SCUBE2 expression and ALP expression (**b**) and NK cell infiltration (**c**). **d**, **e** Effects of oral Sonidegib administration on bone metastasis in BALB/c mice with intracardiac injection of 4T1.2 cells ($n = 9$ per group). Shown are bone metastasis BLI and representative images (**d**) and survival of the mice (**e**). **f** Effects of oral Sonidegib administration from day 7 after orthotopic injection of 4T1.2 cells with *Scube2* overexpression in BALB/c mice ($n = 9$, 8 mice for control and Sonidegib groups, respectively). Shown are normalized BLI quantification of hind limb and representative images. **g** SHH secretion by 4T1.2 cells treated with IgG or the SCUBE2-neutralizing antibody LTMA16D5 (16D5). **h** ALP activity of MSC-derived osteoblasts treated with DMEM medium or CM from MCF7 cells pretreated with LTMA16D5 ($n = 6$ biologically independent samples). **i–l** Efficacy of LTMA16D5 to treat bone metastasis in nude mice with intracardiac injection of MCF7 cells ($n = 9$ mice per group). Shown are normalized BLI quantitation and representative images of whole body bone metastasis (**i**), ex vivo BLI quantification of hind limbs and H&E staining of bone sections (**j**), serological level of human SHH in the mice (**k**), and IF intensities of ALP and NKp46 in bone metastases (**l**, $n = 5$ RMFs from 3 mice per group). *P* values were calculated by two-tailed unpaired *t*-test (**a**, **f**, **h**, **j–l**), Pearson correlation analysis (**b**, **c**) or log-rank test (**e**) and repeated measures two-way ANOVA (**d**, **i**). Scale bars, 100 μm. Data represent mean ± SD (**h**) or mean ± SEM (**d**, **f**, **i–l**).

screening. The antibody purified from hybridoma-inoculated mouse ascites (Supplementary information, Fig. S10d) specifically detected SCUBE2 in lysates of SCUBE2-expressing tumor cells (Supplementary information, Fig. S10e). Importantly, LTMA16D5 effectively inhibited SHH release from 4T1.2 cells (Fig. 8g) and MCF7 cells in a dose-dependent manner (Supplementary information, Fig. S10f), leading to suppression of Hedgehog signaling (Supplementary information, Fig. S10g) and osteoblastogenesis (Fig. 8h) in MSCs when MSCs were cultured in tumoral CM.

Then we further tested the efficacy of LTMA16D5 to treat bone metastasis in vivo. Notably, daily intraperitoneal injection of LTMA16D5 in nude mice with intracardiac implantation of MCF7 cells significantly alleviated mice from bone metastasis burden (Fig. 8i, j). In addition, we observed a reduction of SHH secreted by MCF7 cells in the blood of mice treated with the antibody (Fig. 8k), together with fewer osteoblasts and more NK cells in bone metastases (Fig. 8l; Supplementary information, Fig. S10h). In addition, LTMA16D5 was also effective for metastasis treatment in immunocompetent mice. When the BALB/c mice inoculated with 4T1.2 cells were treated with LTMA16D5 hybridoma CM, suppression of serological murine SHH level and bone metastasis was obviously observed (Supplementary information, Fig. S10i–k). IF analyses of bone sections also showed suppressed osteoblastogenesis and recovered NK infiltration around tumor cells, accompanied by elevated tumor death (Supplementary information, Fig. S10l). Collectively, our data demonstrated the promising potential of the SCUBE2 neutralizing antibody to treat breast cancer bone metastasis.

DISCUSSION

Previous studies have identified a plethora of tumor genetic programs regulating bone metastasis of breast cancer. However, these regulations were primarily established with triple-negative or ER$^-$ cell line models, including MDA-MB-231, 4T1, AT3 cells and their derivatives.[31,83–85] More importantly, many of the tumor-derived molecules reported to promote bone metastasis, such as CXCR4, MMP1, IL6 and Jagged1,[21] are often known to be upregulated in triple-negative breast cancer and thus cannot explain the bone preference of luminal breast cancer metastasis. In this study, we identified the secretory protein SCUBE2 with a critical role in bone colonization of luminal breast cancer. SCUBE2 acts on tumor cells in an autocrine manner to release membrane-anchored SHH, leading to Hedgehog signaling activation and differentiation of osteogenic cells. Osteoblasts secrete collagen to activate the inhibitory LAIR1 signal of NK cells, resulting in

immune suppression and tumor cell survival in bone (Fig. 7j). Importantly, SCUBE2 is a downstream component of ER signaling and therefore specifically upregulated in luminal tumors. Thus, our findings discover a mechanism of high risk for bone recurrence in luminal breast cancer. In addition, the involvement of osteogenic niche in the pathway also explains the unique tropism of luminal tumors to bone, but not to other organs, for metastasis.

Our study will also enrich the understanding towards osteogenic niches in bone metastasis. Tumor cells are known to exploit hematopoietic niches or mesenchymal niches for bone colonization.[86] A number of recent studies[28–32] also demonstrated the role of osteogenic niches in bone colonization of cancer cells. Osteogenic cells can promote tumor colonization by direct tumor contact via adherens junction or gap junction,[28–32] or by secreting pro-tumor inflammatory cytokines.[28–30] In addition, osteoblasts educated by tumor cells can engage osteoclasts to facilitate osteolytic niches.[31,32] Here we report an immune-suppressive role of osteoblast niche. SHH-stimulated osteoblasts deposit collagens in the niches to activate the LAIR1 inhibitory signal of lymphocytes including NK cells, thus creating a protective milieu and shielding tumor cells from immune surveillance. This is particularly important for disseminated tumor cells just arriving at bone. Concordantly, SCUBE2 plays a role mainly in the early colonization stage. These findings will promote the comprehension of dynamic regulation of osteogenic and osteolytic niches in different stages of bone colonization.

Notably, we found that SCUBE2-induced osteogenic niches only sustain tumor survival by immune suppression, but cannot directly promote tumor cell proliferation. This might be in concordance with the clinical observations that bone recurrence of luminal tumors usually has a late onset.[9–12,87] Sustained survival of disseminated luminal tumor cells, which are overall less malignant than those of other subtypes, would result in persistence of residual tumors in bone and late recurrence. This could also reconcile with a previous finding that osteogenic niche contributes to metastatic dormancy of breast cancer in bone,[33] as tumor dormancy is characterized with sustained survival and slowed proliferation.

Noteworthily, ectopically expressed SCUBE2 could also promote bone metastasis in triple-negative cell lines. Therefore, although SCUBE2 is specifically upregulated by ER in luminal tumors, its function may not be dependent on the luminal cell context. This is reasonable, as its downstream signaling components, such as tumoral SHH expression, are not specific to luminal cancer cells. In addition, although we found the osteoblast-dependent effect of SCUBE2 on bone metastasis but not on primary tumor growth, several previous studies reported the roles of SCUBE2 in tumor cell proliferation, migration and invasion.[88–90] Notably, SCUBE2 was shown to both suppress and enhance epithelial-mesenchymal transition in different cancer cells.[88,89] These reports indicated the complex roles of SCUBE2 in tumor progression, which might be dependent on the tumor cell context and microenvironment.

SCUBE2 expression in both tumors and blood is significantly associated with bone metastasis risk, suggesting its prognostic value in luminal cancer. More importantly, our study provides the rationale to target SCUBE2 and its downstream Hedgehog signaling for metastasis treatment. Hedgehog signaling in tumor cells is known to regulate various processes of cancer progression.[79] Our data showed that Hedgehog signaling in stromal cells also contribute to cancer immune regulation and metastasis. Targeting Hedgehog signaling with Sonidegib effectively suppresses bone recurrence of breast cancer, which may greatly broaden the application potential of the candidate drug which is being tested in clinical trials for advanced solid tumor and basal cell carcinoma.[81] In contrast to the ubiquitous expression of Hedgehog ligands and critical role of Hedgehog signaling in development, the highly specific expression pattern of SCUBE2 in luminal cancer cells argues for the therapeutic potential of direct SCUBE2 targeting. The monoclonal neutralizing antibody LTMA16D5 has showed impressive efficacy to inhibit bone metastasis in multiple metastasis models. Although further studies are needed to evaluate the therapeutic potential of the antibody, targeting SCUBE2 might be a promising approach in metastasis treatment.

MATERIALS AND METHODS

Constructs and reagents

Human *SCUBE2* was cloned into pLVX-neo vector (Clontech) and murine *Scube2* and *Gli1* were cloned into pLVX-puro vector (Clontech) for overexpression. The annealed sense and antisense shRNA oligonucleotides were cloned into pLKO.1-puro vector (Addgene) for knockdown of human *SCUBE2*, *SHH* or murine *Smo*, respectively. siRNAs were purchased from GenePharma. For promoter activity analysis, the −2071 to +71 sequence flanking the transcription start site of *SCUBE2* was cloned into pGL3-basic (Promega). The GLI luciferase reporter contains eight repeats of the GLI-binding site (CGACAAGCAGGGAACACCCAAGTAGAAG) in the backbone of pGL3-basic (Promega). Sequences of all shRNAs, siRNAs and primers for qRT-PCR were listed in Supplementary information, Table S1. The antibodies used for western blotting, immunohistochemistry, ELISA, IF and FACS analyses were listed in Supplementary information, Table S2. Chemicals and recombinant proteins, as well as the corresponding concentrations used in in vitro and in vivo assays, were listed in Supplementary information, Table S3.

Cell lines

MDA-MB-231, Py8119 and murine MSCs were grown in DMEM (Gibco, 11965118) with 10% FBIS (Sunrise, SR100180.03) and 100 μg/mL penicillin/streptomycin/fungizone (Gibco, 15240062). MCF7 and 4T1.2 cells were grown in DMEM supplemented with 10% FBS, 100 μg/mL penicillin/streptomycin/fungizone, NEAA (Gibco, 11140050) and Na pyruvate (Gibco, 11360070). T47D cells were grown in PRMI1640 (Gibco, 11875119) supplemented with 10% FBS, 100 μg/mL penicillin/streptomycin/fungizone, 10 mM HEPES (Gibco, 1894147) and 8 μg/mL insulin (Biogems, 10-365-1).

Osteoblastogenesis assays

Human or mouse MSCs were incubated in osteogenic media, α-MEM with 10% FBS and antibiotics supplemented with 100 nM Dexamethasone (Sigma, D4902), 10 mM β-phosphoglycerol (Sigma, G9422), 50 μM L-ascorbic acid (Sigma, A4544). CM from cancer cells were mixed with osteogenic media at a ratio of 1:4 for osteoblast differentiation. Various inhibitors and recombinant proteins were used to treat the cancer cells prior to CM harvest, or administered directly into the CM-osteogenic culture mixture, as specified for each experiment. Fresh media were changed every three days. At day 7, ALP activity was quantified as described before. Briefly, the culture media were removed and cell cultures were washed with PBS and lysed in NP40 protein lysis buffer. 20 μL cell lysate was incubated in 100 μL pNPP substrate solution (0.1 M $NaHCO_3$-$NaCO_3$ (pH 10), 0.1% Triton X-100, 2 mM $MgSO_4$, 6 mM pNPP) for 15 min at 37 °C in dark condition. The enzymatic reaction was stopped by adding 80 μL sodium hydroxide each well and the plate was read at 405 nm in a microplate reader. ALP content was determined by 405 nm absorption over total protein load. ARS staining was performed at day 13 to visualize bone module formation. Cells were washed with PBS, fixed with 4% PFA for 15 min at room temperature, washed twice with excess PBS and stained with 2% ARS (pH 4.1) solution for 20 min with gentle agitation at room temperature. Excess dye was aspirated off and cells were washed 4 times with ddH_2O. Bone nodules, appearing to be red, were visualized under light microscope and photographed. Quantification of ARS area was performed with Image J.

In vitro immune killing assays

To analyze immune killing in vitro, MCF7 cells pre-labeled with luciferase were seeded in a 96-well plate overnight. Jurkat cells were activated by treating with CD3/CD28 (25 μL/mL; Stemcell, 10971) for 24 h prior to killing. NK92 or Jurkat cells were added at a ratio of 1:1 or 5:1 to tumor cells, respectively. CM from osteoblasts accounted for 20%–25% in total medium. For each treatment condition, culture wells with only tumor cells, but not immune cells, were used as control. After co-culturing for

24–48 h, supernatant was discarded and the cells were washed by PBS twice. Cells were lysed by luciferase lysis buffer and luciferase assays were performed to quantitate the surviving cancer cells. Immune killing efficiency of tumor cells was expressed as the signal of immune cell–tumor cell co-cultures divided by the signal of the tumor cell-only cultures.

Organoid killing assays

The PDO sample LTMBC-3 of luminal breast cancer was established as described previously.[91] Briefly, tumor tissues derived from surgical resections were cut into small pieces and enzymatically digested using 5 mg/mL collagenase type I (ThermoFisher, 17100017), 1% Dispase (Roche, 4942078001) and DNAase I (NEB, M0303S) in PBS. Cells were further disassociated with shaking for 30 min at 37 °C, pipette dispelling, 70-μm filtering and 40-μm filtering again. The resulting cells were centrifuged and washed with PBS. Red blood cells were lysed with RBC lysis buffer (Sigma, R7757) for 10 min and then cell numbers were counted before embedding in Matrigel (BD bioscience, 354234). After solidification for 30 min at 37 °C, cells were overlaid with human breast cancer organoid medium, composed of Advanced DMEM/F12 (Gibco) supplemented with 250 ng/mL R-Spondin 3 (R&D, 3500-RS/CF), 5 nM Neuregulin 1 (Peprotech, 100-03), 5 ng/mL FGF 7 (Peprotech, 100-19), 20 ng/mL FGF 10 (Peprotech, 100-26), 5 ng/mL EGF (Peprotech, AF-100-15), 100 ng/mL Noggin (Peprotech, 120-10C), 500 nM A83-01 (Tocris, 2939), 5 mM Y-27632 (Abmole, Y-27632), 500 nM SB202190 (Sigma, S7067), B27 supplement (Gibco, 17504-44), 1.25 mM N-Acetylcysteine (Sigma, A9165-5g), 5 mM Nicotinamide (Sigma, N0636), GlutaMax (Gibco), 10 mM HEPES (Gibco), 100 mg/mL Penicillin/Streptomycin (Hyclone) and 50 mg/mL Primocin (Invivogen, Ant-pm-1). In vitro organoid killing assay was performed as described.[92] Briefly, organoids were isolated from culture dishes and washed with PBS twice to remove Matrigel. Part of the organoids were dissociated to single cells by TrypLE Express (ThermoFisher, 12604021) and cell numbers were counted using a hemocytometer, to infer the number of tumor cells per tumor organoid to allow co-culture of organoids and NK cells at a 1:1 ratio. To facilitate visualization, organoids were stained with CFSE (MCE, HY-D0938) for 5 min and washed with PBS for three times, resuspended in T cell medium and seeded with indicated cells. After 3 days of co-culture, fluorescence images were taken and analyzed with Image J.

Isolation of bone cells

To obtain bone niche cells for scRNA-seq or FACS analysis, mice were sacrificed and bone digestion was performed as previously described.[93,94] Briefly, bones (femur and tibia) were harvested and placed in Media 199 (BasalMedia, L640KJ) supplemented with 2% FBS. After removal of muscle and tendon tissues, bones were cut and gently crushed into small fragments and digested with 2.2 mg/mL collagenase II (Sigma, C6885) in M199 media for 50 min, at 37 °C with agitation. After digestion, fractions were filtered through a 70-μm filter followed by a 40-μm filter. Cells were centrifuged (200× *g*, 10 min) and washed with PBS twice. Erythrocytes were lysed in RBC lysis buffer (BD, 555899) for 5 min on ice.

FACS analyses

Intracellular cytokine staining was performed as previously described.[95] After isolation of bone cells, cells were counted and treated with cell stimulation cocktail plus protein transport inhibitors (eBioscience, 00-4975-93) in M199 media supplemented with 10% FBS for 5 h. FcR was blocked by the CD16/CD32 antibody (BD Life Sciences, 2.4G2) at the concentration of 0.5 mg per million cells before antibody staining. After surface staining for 1 h at room temperature in the dark, cells were washed with FACS buffer (PBS with 10% FBS) three times and fixed with IC fixation buffer (Invitrogen, 00-8222) for 30 min at 4 °C. Cells were washed and permeabilized with permeabilization buffer (Invitrogen, 00-8333). Next, cells were stained with intracellular staining cocktail for 30 min at room temperature. Cells were washed and resuspended in FACS buffer. FACS was performed with a CytoFLEX LX (Beckman) FACS system and quantified by the CytExpert software. The gating strategies for various cell types were shown in Supplementary information, Fig. S11.

RNA-seq and scRNA-seq analyses

RNA sequencing of MSCs was performed as previously described.[96] Briefly, total RNAs of MSCs and MSC-derived osteoblasts were extracted by TRIzol reagent (Invitrogen, 15596018). Library construction and sequencing were performed at WuXi NextCODE, Shanghai with an Illumina's standard protocol. Raw reads were filtered and aligned to the reference sequences using STAR (v2.4.2a). Genes with fold changes > 2 and P value < 0.05 were selected as significantly differentially expressed genes.

For scRNA-seq analysis, cells were isolated from bone marrow of long bones of the mice and sorted with CD45 mouse microbeads (Miltenyi Biotec, 5211005943) to enrich $CD45^-$ stromal cells or to isolate $CD45^+$ immune cells. Effluents were collected and centrifuged at 200× *g* for 10 min. Library construction and sequencing were performed at Shanghai Biotechnology Corporation. Single-cell libraries were generated using the Chromium Next GEM Single Cell 3′ Reagent Kits v3.1 (10× Genomics) according to the manufacturer's instructions. After sequencing, FASTQ files were converted to cell expression matrices by aligning to the mouse genome (version mm10) with Cell Ranger count (version 2.0.1, 10× Genomics). For $CD45^-$ cell analysis, we captured 9359 cells with a mean of 72,767 read counts and a median of 2201 genes per cell in control group, and 8871 cells with a mean of 73,544 read counts and a median of 2595 genes per cell in *SCUBE2*-knockdown group. For $CD45^+$ cell analysis, we captured 5008 cells with a mean of 11,5361 read counts and a median of 1268 genes per cell in control group, and 8560 cells with a mean of 58,506 read counts and a median of 1537 genes per cell in *SCUBE2*-knockdown group.

Quantification of osteoblasts in the microenvironment niche

Quantification of osteoblasts was performed as previously described.[29] Briefly, microenvironment niche cells were defined as cells immediately adjacent to micrometastases and in direct contact with tumor cells. ALP^+ osteoblasts and all non-tumor in the niches were counted. Percentages of ALP^+ osteoblasts of all niche cells were calculated.

Luciferase assay

T47D or MC3T3 cells were transfected with the denoted constructs and starved overnight in serum-free DMEM. Cells were then treated in triplicates with the indicated factors in serum-free DMEM for 36 h. Afterwards, cells were rinsed with PBS and lysed by luciferase lysis buffer (2 mM EDTA, 20 mM DTT, 10% glycerol, 1% Triton X-100 and 25 mM Tris-base, pH 7.8) at room temperature for 1 h with shaking. The resultant lysate was added with firefly (25 mM glycyglycine, 15 mM potassium phosphate, 15 mM $MgSO_4$, 2 mM ATP, 10 mM DTT and 1 mM D-luciferin, pH 7.8) and Renilla (0.5 M NaCl, 1 mM EDTA, 0.1 M potassium phosphate, 0.04% BSA and 2 μM coelenterazine, pH 7.4) luciferase assay buffer, respectively. Renilla activity reads were used for normalization.

Neutralizing antibody production and purification

SCUBE2 neutralizing mono-antibody was developed by Abclonal Technology. Briefly, mice were immunized with the CUB domain peptide of SCUBE2. Splenocytes of immunized mice were separated and fused with SP20 tumor cells. Hybridoma were cultured with HybGro media (BasalMedia, H630KJ) supplemented with CellTurbo (BasalMedia, H460JV). Neutralizing analysis of hybridoma supernatants was performed by competitive ELISA with SHH. For neutralizing antibody production, female BALB/c mice were injected with 300 μL pristane (Sigma, P9622). 2×10^6 hybridoma cells were injected intraperitoneally 7 days after pristane injection. After 7–14 days, mice were sacrificed and ascites were collected. Antibody purification was performed with Protein G resin (Sangon Biotech, C600991). Purified antibodies were dialyzed into PBS and concentrated to 1 mg/mL for in vitro and in vivo use. Antibody isotyping was performed with mouse mono-antibody isotyping ELISA kit (Proteintech, PK20003) according to the manufacturer's instruction. Briefly, purified antibody was diluted to 200 ng/mL and 50 μL diluted antibody was incubated with 50 μL goat anti-mouse IgA/IgM/IgG-HRP in each well for 1 h at room temperature. After three washes with washing buffer, signals were detected using TMB solution and read at 450 nm.

Mouse experiments

Female BALB/c, C57 and athymic mice (6–8-week-old) were used in all animal experiments. Orthotopic, intracardiac and intra-iliac artery injection were performed as previously described.[23,29] Briefly, 1×10^5, 1×10^5 and 4×10^5 luciferase-labeled tumor cells were injected into the fat pad, left ventricle and iliac artery for primary tumor and bone metastasis analyses, respectively. For experiments involving human luminal breast cancer cells, mice were subcutaneously injected with 3.75 mg/kg estradiol valerate every other day (Selleck, S3149) as described previously.[97] 50 mg/kg Sonidegib (Abmole, LED225) and dimethylsulfoxide control were orally

administered daily until the mice were sacrificed. For LTMA16D5 hybridoma CM treatment, HybGro medium (BasalMedia, H630KJ) control or hybridoma CM were injected intravenously every day until the mice were sacrificed. For LTMA16D5 antibody treatment, IgG (100 μg per mouse; YEASEN, 36111ES60) or purified LTMA16D5 antibody (100 μg per mouse) was intraperitoneally injected daily until the mice were sacrificed. BLI was acquired with a NightOWL II LB983 Imaging System (Berthold). Day 0 signal was collected immediately after tumor cell inoculation and applied for BLI signal normalization. All animal studies were conducted according to the guidelines for the care and use of laboratory animals and were approved by the Institutional Animal Care and Use Committee of Shanghai Institute of Nutrition and Health.

Clinical analysis

Frozen primary tumor specimens, serum samples and paraffin-embedded bone metastasis specimens of breast cancer, as well as the PDO breast cancer samples, were obtained from Qilu Hospital of Shandong University, with informed consent from all subjects and approval from the Institutional Research Ethics Committee of Qilu Hospital (reference no. KYLL-2016-255). The clinical information of the samples was provided in Supplementary information, Table S4. For each sample, SCUBE2, ALP and COL1 were scored as low expression (negative/low) or high expression (medium/high) according to the staining intensities. Serum samples were pre-treated according to the manufacturer's instructions and analyzed with ELISA kits for SCUBE2.

The reported breast cancer clinical datasets (GSE2034, GSE5327, GSE12276 and GSE2603) were combined into a merged Erasmus/MSK cohort, as done in a previous study,[48] to increase the sample sizes for analysis of organotropism-associated genes. Differentially expressed genes encoding secretory proteins were analyzed between luminal vs TN subtype or bone-metastatic and lung-metastatic patients by student's *t*-test analysis, with cutoffs of P values < 0.01 and fold changes > 2. These genes were further ranked by the relative fold changes.

Statistical analyses

Data analyses were performed using GraphPad Prism 7.0 (GraphPad Software, La Jolla, CA, USA). The data presentation and statistical analyses are described in the figure legends. P values < 0.05 were considered as statistically significant.

DATA AVAILABILITY

The sequence data of osteoblasts were deposited in the National Omics Data Encyclopedia (NODE) with the primary accession number OEP002689. Original data of all figures were deposited in Mendeley Data (https://data.mendeley.com/v1/datasets/jkpn67jwsd/draft?preview=1). Other data of this study are available from the corresponding author upon reasonable request.

REFERENCES

1. Zlotnik, A., Burkhardt, A. M. & Homey, B. Homeostatic chemokine receptors and organ-specific metastasis. *Nat. Rev. Immunol.* **11**, 597–606 (2011).
2. Roodman, G. D. Mechanisms of bone metastasis. *N. Engl. J. Med.* **350**, 1655–1664 (2004).
3. Weilbaecher, K. N., Guise, T. A. & McCauley, L. K. Cancer to bone: a fatal attraction. *Nat. Rev. Cancer* **11**, 411–425 (2011).
4. Coleman, R. E. et al. Bone metastases. *Nat. Rev. Dis. Primers* **6**, 83 (2020).
5. Perou, C. M. et al. Molecular portraits of human breast tumours. *Nature* **406**, 747–752 (2000).
6. Sorlie, T. et al. Repeated observation of breast tumor subtypes in independent gene expression data sets. *Proc. Natl. Acad. Sci. USA* **100**, 8418–8423 (2003).
7. Sorlie, T. et al. Gene expression patterns of breast carcinomas distinguish tumor subclasses with clinical implications. *Proc. Natl. Acad. Sci. USA* **98**, 10869–10874 (2001).
8. Rouzier, R. et al. Breast cancer molecular subtypes respond differently to preoperative chemotherapy. *Clin. Cancer Res.* **11**, 5678–5685 (2005).
9. Smid, M. et al. Subtypes of breast cancer show preferential site of relapse. *Cancer Res.* **68**, 3108–3114 (2008).
10. Savci-Heijink, C. D. et al. Retrospective analysis of metastatic behaviour of breast cancer subtypes. *Breast Cancer Res. Treat.* **150**, 547–557 (2015).
11. Kunikullaya, S. U., Poddar, J., Sharma, A. D. & Patel, S. Pattern of distant metastasis in molecular subtypes of carcinoma breast: An institutional study. *Indian J. Cancer* **54**, 327–332 (2017).
12. Kennecke, H. et al. Metastatic behavior of breast cancer subtypes. *J. Clin. Oncol.* **28**, 3271–3277 (2010).
13. Farach-Carson, M. C., Lin, S. H., Nalty, T. & Satcher, R. L. Sex differences and bone metastases of breast, lung, and prostate cancers: do bone homing cancers favor feminized bone marrow? *Front. Oncol.* **7**, 163 (2017).
14. Lee, S. J. et al. Implications of bone-only metastases in breast cancer: favorable preference with excellent outcomes of hormone receptor positive breast cancer. *Cancer Res. Treat.* **43**, 89–95 (2011).
15. Wang, J., Jarrett, J., Huang, C. C., Satcher, R. L. Jr. & Levenson, A. S. Identification of estrogen-responsive genes involved in breast cancer metastases to the bone. *Clin. Exp. Metastasis* **24**, 411–422 (2007).
16. Wei, S., Li, Y., Siegal, G. P. & Hameed, O. Breast carcinomas with isolated bone metastases have different hormone receptor expression profiles than those with metastases to other sites or multiple organs. *Ann. Diagn. Pathol.* **15**, 79–83 (2011).
17. Onishi, T., Hayashi, N., Theriault, R. L., Hortobagyi, G. N. & Ueno, N. T. Future directions of bone-targeted therapy for metastatic breast cancer. *Nat. Rev. Clin. Oncol.* **7**, 641–651 (2010).
18. Zhang, X. H. et al. Latent bone metastasis in breast cancer tied to Src-dependent survival signals. *Cancer Cell* **16**, 67–78 (2009).
19. Hayashi, N. et al. Bone metastasis-related signaling pathways in breast cancers stratified by estrogen receptor status. *J. Cancer* **8**, 1045–1052 (2017).
20. Mundy, G. R. Metastasis to bone: causes, consequences and therapeutic opportunities. *Nat. Rev. Cancer* **2**, 584–593 (2002).
21. Ell, B. & Kang, Y. SnapShot: bone metastasis. *Cell* **151**, 690.e1 (2012).
22. Suva, L. J., Washam, C., Nicholas, R. W. & Griffin, R. J. Bone metastasis: mechanisms and therapeutic opportunities. *Nat. Rev. Endocrinol.* **7**, 208–218 (2011).
23. Zhuang, X. et al. Differential effects on lung and bone metastasis of breast cancer by Wnt signalling inhibitor DKK1. *Nat. Cell Biol.* **19**, 1274–1285 (2017).
24. Coleman, R. E. Zoledronic acid ameliorates the effects of endocrine therapy on bone health in women with early-stage breast cancer. *Nat. Clin. Pract. Endocrinol. Metab.* **5**, 72–73 (2009).
25. Mackiewicz-Wysocka, M., Pankowska, M. & Wysocki, P. J. Progress in the treatment of bone metastases in cancer patients. *Expert Opin. Investig. Drugs* **21**, 785–795 (2012).
26. Haider, M. T., Holen, I., Dear, T. N., Hunter, K. & Brown, H. K. Modifying the osteoblastic niche with zoledronic acid in vivo-Potential implications for breast cancer bone metastasis. *Bone* **66**, 240–250 (2014).
27. Devignes, C. S. et al. HIF signaling in osteoblast-lineage cells promotes systemic breast cancer growth and metastasis in mice. *Proc. Natl. Acad. Sci. USA* **115**, E992–E1001 (2018).
28. Bussard, K. M., Venzon, D. J. & Mastro, A. M. Osteoblasts are a major source of inflammatory cytokines in the tumor microenvironment of bone metastatic breast cancer. *J. Cell. Biochem.* **111**, 1138–1148 (2010).
29. Wang, H. et al. The osteogenic niche promotes early-stage bone colonization of disseminated breast cancer cells. *Cancer Cell* **27**, 193–210 (2015).
30. Wang, H. et al. The osteogenic niche is a calcium reservoir of bone micrometastases and confers unexpected therapeutic vulnerability. *Cancer Cell* **34**, 823–839.e7 (2018).
31. Zheng, H. et al. Therapeutic antibody targeting tumor- and osteoblastic niche-derived jagged1 sensitizes bone metastasis to chemotherapy. *Cancer Cell* **32**, 731–747.e6 (2017).
32. Sethi, N., Dai, X., Winter, C. G. & Kang, Y. Tumor-derived JAGGED1 promotes osteolytic bone metastasis of breast cancer by engaging notch signaling in bone cells. *Cancer Cell* **19**, 192–205 (2011).
33. Kolb, A. D., Shupp, A. B., Mukhopadhyay, D., Marini, F. C. & Bussard, K. M. Osteoblasts are "educated" by crosstalk with metastatic breast cancer cells in the bone tumor microenvironment. *Breast Cancer Res.* **21**, 31 (2019).
34. Grimmond, S. et al. Cloning, mapping, and expression analysis of a gene encoding a novel mammalian EGF-related protein (SCUBE1). *Genomics* **70**, 74–81 (2000).
35. Kawakami, A. et al. The zebrafish-secreted matrix protein you/scube2 is implicated in long-range regulation of hedgehog signaling. *Curr. Biol.* **15**, 480–488 (2005).
36. Johnson, J. L. et al. Scube activity is necessary for Hedgehog signal transduction in vivo. *Dev. Biol.* **368**, 193–202 (2012).
37. Woods, I. G. & Talbot, W. S. The you gene encodes an EGF-CUB protein essential for Hedgehog signaling in zebrafish. *PLoS Biol.* **3**, e66 (2005).
38. Creanga, A. et al. Scube/You activity mediates release of dually lipid-modified Hedgehog signal in soluble form. *Genes Dev.* **26**, 1312–1325 (2012).
39. Parchure, A., Vyas, N. & Mayor, S. Wnt and Hedgehog: secretion of lipid-modified morphogens. *Trends Cell Biol.* **28**, 157–170 (2018).
40. Jakobs, P. et al. Scube2 enhances proteolytic Shh processing from the surface of Shh-producing cells. *J. Cell Sci.* **127**, 1726–1737 (2014).

41. Wierbowski, B. M. et al. Hedgehog pathway activation requires coreceptor-catalyzed, lipid-dependent relay of the Sonic Hedgehog ligand. *Dev. Cell* **55**, 450–467. e8 (2020).
42. Tukachinsky, H., Kuzmickas, R. P., Jao, C. Y., Liu, J. & Salic, A. Dispatched and scube mediate the efficient secretion of the cholesterol-modified hedgehog ligand. *Cell Rep.* **2**, 308–320 (2012).
43. Tsai, M. T. et al. Isolation and characterization of a secreted, cell-surface glycoprotein SCUBE2 from humans. *Biochem. J.* **422**, 119–128 (2009).
44. Petrov, K., Wierbowski, B. M., Liu, J. & Salic, A. Distinct cation gradients power cholesterol transport at different key points in the Hedgehog signaling pathway. *Dev. Cell* **55**, 314–327.e317 (2020).
45. Smid, M. et al. Genes associated with breast cancer metastatic to bone. *J. Clin. Oncol.* **24**, 2261–2267 (2006).
46. Minn, A. J. et al. Genes that mediate breast cancer metastasis to lung. *Nature* **436**, 518–524 (2005).
47. Wang, Y. et al. Gene-expression profiles to predict distant metastasis of lymph-node-negative primary breast cancer. *Lancet* **365**, 671–679 (2005).
48. Bos, P. D. et al. Genes that mediate breast cancer metastasis to the brain. *Nature* **459**, 1005–1009 (2009).
49. Minn, A. J. et al. Lung metastasis genes couple breast tumor size and metastatic spread. *Proc. Natl. Acad. Sci. USA* **104**, 6740–6745 (2007).
50. Cancer Genome Atlas, N. Comprehensive molecular portraits of human breast tumours. *Nature* **490**, 61–70 (2012).
51. Richardson, A. L. et al. X chromosomal abnormalities in basal-like human breast cancer. *Cancer Cell* **9**, 121–132 (2006).
52. Lelekakis, M. et al. A novel orthotopic model of breast cancer metastasis to bone. *Clin. Exp. Metastasis* **17**, 163–170 (1999).
53. Paul, F. et al. Transcriptional heterogeneity and lineage commitment in myeloid progenitors. *Cell* **163**, 1663–1677 (2015).
54. Tusi, B. K. et al. Population snapshots predict early haematopoietic and erythroid hierarchies. *Nature* **555**, 54–60 (2018).
55. Nikolic, T., Dingjan, G. M., Leenen, P. J. & Hendriks, R. W. A subfraction of B220(+) cells in murine bone marrow and spleen does not belong to the B cell lineage but has dendritic cell characteristics. *Eur. J. Immunol.* **32**, 686–692 (2002).
56. Giladi, A. et al. Single-cell characterization of haematopoietic progenitors and their trajectories in homeostasis and perturbed haematopoiesis. *Nat. Cell Biol.* **20**, 836–846 (2018).
57. Wiraja, C., Yeo, D. C., Chong, M. S. & Xu, C. Nanosensors for continuous and noninvasive monitoring of mesenchymal stem cell osteogenic differentiation. *Small* **12**, 1342–1350 (2016).
58. Corada, M. et al. Monoclonal antibodies directed to different regions of vascular endothelial cadherin extracellular domain affect adhesion and clustering of the protein and modulate endothelial permeability. *Blood* **97**, 1679–1684 (2001).
59. Lin, Y. C. et al. Endothelial SCUBE2 interacts With VEGFR2 and regulates VEGF-induced angiogenesis. *Arterioscler. Thromb. Vasc. Biol.* **37**, 144–155 (2017).
60. Huang, W., Yang, S., Shao, J. & Li, Y. P. Signaling and transcriptional regulation in osteoblast commitment and differentiation. *Front. Biosci.* **12**, 3068–3092 (2007).
61. Greenbaum, A. et al. CXCL12 in early mesenchymal progenitors is required for haematopoietic stem-cell maintenance. *Nature* **495**, 227–230 (2013).
62. Kim, W. K., Meliton, V., Bourquard, N., Hahn, T. J. & Parhami, F. Hedgehog signaling and osteogenic differentiation in multipotent bone marrow stromal cells are inhibited by oxidative stress. *J. Cell Biochem.* **111**, 1199–1209 (2010).
63. Li, L. et al. Hedgehog signaling is involved in the BMP9-induced osteogenic differentiation of mesenchymal stem cells. *Int. J. Mol. Med.* **35**, 1641–1650 (2015).
64. Zhao, Q. et al. Identification of genes expressed with temporal-spatial restriction to developing cerebellar neuron precursors by a functional genomic approach. *Proc. Natl. Acad. Sci. USA* **99**, 5704–5709 (2002).
65. Yauch, R. L. et al. A paracrine requirement for hedgehog signalling in cancer. *Nature* **455**, 406–410 (2008).
66. Bonnans, C., Chou, J. & Werb, Z. Remodelling the extracellular matrix in development and disease. *Nat. Rev. Mol. Cell. Biol.* **15**, 786–801 (2014).
67. Kaur, A. et al. Remodeling of the collagen matrix in aging skin promotes melanoma metastasis and affects immune cell motility. *Cancer Discov.* **9**, 64–81 (2019).
68. Egeblad, M., Rasch, M. G. & Weaver, V. M. Dynamic interplay between the collagen scaffold and tumor evolution. *Curr. Opin. Cell. Biol.* **22**, 697–706 (2010).
69. Meyaard, L. et al. LAIR-1, a novel inhibitory receptor expressed on human mononuclear leukocytes. *Immunity* **7**, 283–290 (1997).
70. Meyaard, L. The inhibitory collagen receptor LAIR-1 (CD305). *J. Leukoc. Biol.* **83**, 799–803 (2008).
71. Lebbink, R. J. et al. Collagens are functional, high affinity ligands for the inhibitory immune receptor LAIR-1. *J. Exp. Med.* **203**, 1419–1425 (2006).
72. Peng, D. H. et al. Collagen promotes anti-PD-1/PD-L1 resistance in cancer through LAIR1-dependent CD8(+) T cell exhaustion. *Nat. Commun.* **11**, 4520 (2020).
73. Rygiel, T. P., Stolte, E. H., de Ruiter, T., van de Weijer, M. L. & Meyaard, L. Tumor-expressed collagens can modulate immune cell function through the inhibitory collagen receptor LAIR-1. *Mol. Immunol.* **49**, 402–406 (2011).
74. Kuczek, D. E. et al. Collagen density regulates the activity of tumor-infiltrating T cells. *J. Immunother. Cancer* **7**, 68 (2019).
75. Boraschi-Diaz, I. et al. Collagen type I degradation fragments act through the collagen receptor LAIR-1 to provide a negative feedback for osteoclast formation. *Bone* **117**, 23–30 (2018).
76. Theocharis, A. D., Skandalis, S. S., Gialeli, C. & Karamanos, N. K. Extracellular matrix structure. *Adv. Drug Deliv. Rev.* **97**, 4–27 (2016).
77. Lebbink, R. J. et al. Mouse leukocyte-associated Ig-like receptor-1 (mLAIR-1) functions as an inhibitory collagen-binding receptor on immune cells. *Int. Immunol.* **19**, 1011–1019 (2007).
78. Jansen, C. A. et al. Regulated expression of the inhibitory receptor LAIR-1 on human peripheral T cells during T cell activation and differentiation. *Eur. J. Immunol.* **37**, 914–924 (2007).
79. Rubin, L. L. & de Sauvage, F. J. Targeting the Hedgehog pathway in cancer. *Nat. Rev. Drug Discov.* **5**, 1026–1033 (2006).
80. Takebe, N. et al. Targeting Notch, Hedgehog, and Wnt pathways in cancer stem cells: clinical update. *Nat. Rev. Clin. Oncol.* **12**, 445–464 (2015).
81. Sekulic, A. & Hoff, Von D. Hedgehog pathway inhibition. *Cell* **164**, 831 (2016).
82. Cortes, J. E., Gutzmer, R., Kieran, M. W. & Solomon, J. A. Hedgehog signaling inhibitors in solid and hematological cancers. *Cancer Treat. Rev.* **76**, 41–50 (2019).
83. Haley, H. R. et al. Enhanced bone metastases in skeletally immature mice. *Tomography* **4**, 84–93 (2018).
84. Eckhardt, B. L. et al. Genomic analysis of a spontaneous model of breast cancer metastasis to bone reveals a role for the extracellular matrix. *Mol. Cancer Res.* **3**, 1–13 (2005).
85. Kang, Y. et al. A multigenic program mediating breast cancer metastasis to bone. *Cancer Cell* **3**, 537–549 (2003).
86. Olechnowicz, S. W. & Edwards, C. M. Contributions of the host microenvironment to cancer-induced bone disease. *Cancer Res.* **74**, 1625–1631 (2014).
87. Kim, R. S. et al. Dormancy signatures and metastasis in estrogen receptor positive and negative breast cancer. *PLoS One* **7**, e35569 (2012).
88. Chen, J. H. et al. Upregulated SCUBE2 expression in breast cancer stem cells enhances triple negative breast cancer aggression through modulation of notch signaling and epithelial-to-mesenchymal transition. *Exp. Cell Res.* **370**, 444–453 (2018).
89. Lin, Y. C., Lee, Y. C., Li, L. H., Cheng, C. J. & Yang, R. B. Tumor suppressor SCUBE2 inhibits breast-cancer cell migration and invasion through the reversal of epithelial-mesenchymal transition. *J. Cell Sci.* **127**, 85–100 (2014).
90. Cheng, C. J. et al. SCUBE2 suppresses breast tumor cell proliferation and confers a favorable prognosis in invasive breast cancer. *Cancer Res.* **69**, 3634–3641 (2009).
91. Cong, M. et al. MTSS1 suppresses mammary tumor-initiating cells by enhancing RBCK1-mediated p65 ubiquitination. *Nat. Cancer* **1**, 222–234 (2020).
92. Dijkstra, K. K. et al. Generation of tumor-reactive T cells by co-culture of peripheral blood lymphocytes and tumor organoids. *Cell* **174**, 1586–1598.e12 (2018).
93. Ambrosi, T. H. et al. Aged skeletal stem cells generate an inflammatory degenerative niche. *Nature* **597**, 256–262 (2021).
94. Baryawno, N. et al. A cellular taxonomy of the bone marrow stroma in homeostasis and leukemia. *Cell* **177**, 1915–1932.e16 (2019).
95. Gupta, S. & Maecker, H. Intracellular cytokine staining (ICS) on human lymphocytes or peripheral blood mononuclear cells (PBMCs). *Bio. Protoc.* **5**, e1442 (2015).
96. Zhang, P. et al. SH3RF3 promotes breast cancer stem-like properties via JNK activation and PTX3 upregulation. *Nat. Commun.* **11**, 2487 (2020).
97. Fleming, J. M., Miller, T. C., Meyer, M. J., Ginsburg, E. & Vonderhaar, B. K. Local regulation of human breast xenograft models. *J. Cell. Physiol.* **224**, 795–806 (2010).

ACKNOWLEDGEMENTS

We would like to thank Kai Wang, Shuyang Yan, Xiang Miao, Yiting Yuan, Jun Li, Zhonghui Weng, Yujia Zhai, Yifan Bu from Institutional Center for Shared Technologies and Facilities of SINH, CAS for technical assistance. The study was funded by the National Natural Science Foundation of China (82230096, 82003090), the National Key R&D Program of China (2020YFA0112300), the Science and Technology Commission of Shanghai Municipality (19JC1416100) and the Youth Innovation Promotion Association of Chinese Academy of Sciences.

AUTHOR CONTRIBUTIONS

G.H. supervised this work. Q.W. and G.H. drafted the manuscript. Q.W., P.T., D.H., Z.J., Y.H., W.L., X.L., Y.W., P.Z. and Y.L. performed the experiments. W.Z., P.S., J.Q., Y.-Z.J.,

Z.-M.S. and Q.Y. contributed to clinical sample collection and analyses. All authors discussed the results and commented on the manuscript.

COMPETING INTERESTS

The authors declare no competing interests.

ADDITIONAL INFORMATION

Supplementary information The online version contains supplementary material available at https://doi.org/10.1038/s41422-023-00810-6.

Correspondence and requests for materials should be addressed to Qifeng Yang or Guohong Hu.